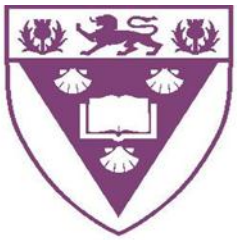

RHODES UNIVERSITY

Grahamstown • 6140 • South Africa

Ore Distribution Controls of the Navachab Gold Mine, Damara Belt, Karibib District, Namibia

---

By

WL Slabbert

A dissertation submitted in partial fulfillment of the requirements for the degree of

MASTER OF SCIENCE

(Exploration Geology)

November 2013

Acknowledgements

I would like to sincerely thank Navachab Gold Mine for all the technical, logistical and financial support which without my participation to the MSc program would not have been possible. I would especially like to thank Graham Bell, Patrick Chizabulyo, Leigh Liebenberg, Richard Manyanga and the whole core-yard staff for their diligent help and support in this regard.

Frik Badenhorst, for your support, motivation, critic discussions and key eye for detail. This study would not have been possible without your guidance and help!

The program director, Professor Yong Yao, is thanked for his academic contributions in making the program relevant and meaningful to industry.

The administrator of the MSc program, Mrs. Ashley Goddard deserves a massive thank you for all the miracles she performs behind the scenes as she keeps the program running smoothly.

I would like to thank my family and friends for always supporting me in achieving my goals as you provided me with the toolset to succeed.

This study is dedicated to my parents!

Declaration

I, Wynand Leon Slabbert declare this dissertation to be my own work. It is submitted in fulfillment of the Degree of Master of Science at the University of Rhodes. It has not been submitted before for any degree or examination in any other University or tertiary institution.

Signature of the candidate: …… 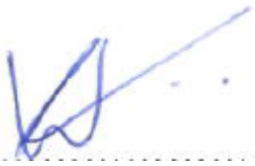 …….

Date: ……18th September 2014……

Abstract

The Navachab Gold mine, an orogenic lode gold deposit, is located in the Karibib region of the Pan-African (ca. 550-500) Damara belt of central Namibia. Gold mineralisation is developed within the steeply NW dipping limb of the Karibib dome. Here, ore envelopes trend along three main orientations: a) trends shallowly towards the NE (the down plunge extent), b) trends sub-vertically in and along the down plunge extent and c) trends sub-horizontally across the down plunge extent. The down plunge extent represents the bulk of the gold mineralisation, hosting the only high grade ores mined at Navachab. As such, past work primarily focused on establishing the controls to the mineralisation observed here. The sub-vertical and sub–horizontal ore trends are seen as secondary, lower grade, being hosted in the footwall. By cutting pushbacks into the footwall, in an effort to regain access to high grade pit bottom, future gold production almost exclusively relies upon optimally mining these ores. This underlines the importance to investigate and outline the mineralising controls to the secondary ore trends.

This study identified the following prevailing quartz vein sets developed within the footwall, set (1) dips shallowly towards the NE (conjugate vein set), (2) steeply towards the NW (bedding parallel veins) and (3) steeply towards the SE (S2 foliation parallel). The NW and SE dipping sets contain high average gold grades, occurring at an infrequent vein density. The NE dipping veins, as a result of occurrence density alone, was highlighted as the dominant gold hosting set. Veining occurred during the late stages of the NW-SE directed, sub-horizontal shortening (D2) event and is associated

with top-to-the-NW thrusting and NW-verging folds. Re-Os molybdenite dating from auriferous quartz veins indicates mineralisation occurred at 525-520 Ma.
As crustal shortening amplified the Karibib dome, flexural flow developed fractures along bedding planes, providing the control to bedding parallel veins (NW dipping). With continued crustal compression the dome later experienced fold lock up associated with reduced mean rock stress and sub-horizontal extension occurred along the steeply NW dipping limb. Horizontal extensional gashes sucked in fluids to form the shallowly NE dipping conjugate vein set. These features suggest the regional D2 strain as the first-order control to quartz vein development, down plunge and within the footwall ores.

To further define the secondary ores, lithological and structural controls were evaluated on a more detailed local scale. With equal amounts of biotite schist and calc-silicate host rock (bulk of the footwall lithology) material analysed, the biotite schist units were found to contain a larger volume amount of quartz veins. The mineralisation incurred is also developed at higher average gold grades compared to that of the calc-silicates, demonstrating biotite schist having the optimal rheology for quartz vein emplacement. Normal faulting and thrusting occurs widespread, at all scale levels, across the footwall. These were primarily observed along bedding foliations and secondly at higher angles cutting across foliation. The study did not constrain the extent of these, but can conclude faulting plays a very prominent role in re-distributing the secondary ores parallel to bedding along sub-vertical trend planes. Great care should be placed in properly modelling these with 3D software such as Leapfrog.

The Navachab gold mineralisation came about as a result of convergent and collisional tectonics activating metamorphic dehydration of the crustal metapelites. As these fluids ascended they absorbed gold from the crust, emplaced by either a magmatic or paleo-placer source. The gold enriched hydrothermal fluids amalgamated in large scale 1ste order structures (shearing of the steep NW limb of the Karibib Dome, the Mon Repos Thrust Zone) that acted as primary active fluid path ways. In the case of Navachab the gold enriched fluid fluxed along these pathways while interacting with fluid sinks related to a physical throttle (brittle schist, folding, bedding parallel shears) and/or a chemical trap (marbles). By summarising and detailing the fluid sinks and active fluid pathways identified by this and previous works, it is strongly recommended that a mineral approach system be designed and implemented as targeting model to lead future exploration endeavours.

Contents

Acknowledgements ii
Declaration iii
Abstract iv
Contents vii
List of Figures ix
List of Tables xii
Chapter 1: Introduction 1
1.1 Locality 1
1.2 Background and Rationale 3
1.3 Aims of the study 5
1.4 Methodology 7
Chapter 2: Regional Geology 9
2.1 Introduction 9
2.2 Evolution of the Damara Belt 13
2.3 Structural Setting of the sCZ 16
2.4 Metamorphism 18
2.5 Lithostratigraphy 19
2.5.1 Abbabis Metamorphic Complex (AMC) 19
2.5.2 Nosib Group 20
2.5.2.1 Etusis Formation 20
2.5.3 Swakop Group 20
2.5.3.1 Chuos Formation 20
2.5.3.2 Spes Bona Formation 21
2.5.3.3 Okawayo Formation 21
2.5.3.4 Oberwasser Formation 22
2.5.3.5 Karibib Formation 22
2.5.3.6 Kuiseb Formation 23
2.6 Intrusive Rocks 23
2.6.1 Pegmatites and Aplites 23
2.6.2 Mafic Rocks 23
2.6.3 Syn- to post-tectonic granitoids 24
2.7 Geochronology 24
Chapter 3: Mine Geology 27

3.1 Introduction 27
3.2 Lithology of the Navachab Open Cast Pit 28
3.2.1 The Spes Bona Formation 30
3.2.2 The Okawayo Formation 32
3.2.3 The Oberwasser Formation 32
3.2.4 Intrusive rocks 32
3.3 Structural Geology of the Navachab Open Cast Pit 33
3.4 Quartz veins in the Footwall 37
3.4.1 Quartz Vein Geometry 39
3.4.2 Quartz vein morphology 44
3.5 Mineralization Evolution 48
3.6 Footwall Ore Distribution 50
3.6.1 Mineralization within different host rocks 51
3.6.2 Mineralization within different quartz vein sets 54
Chapter 4: Discussion 59
Ore distribution 61
The sub-horizontal ore trend 61
The sub-vertical ore trend 62
Additional control 63
Mineralisation Model 63
Chapter 5: Conclusion 66
Host Rock 66
Quartz Vein Sets 66
Displacement 67
Summary of the mineralization controls 67
Recommendations 68
Chapter 6: Reference List 72

List of Figures

Figure 1: Location of the Navachab Gold Mine, situated 10km SW from Karibib on the NW limb of the Karibib Dome (Google Earth). 1

Figure 2: Location of the NGM within the main tectonostratigraphic zones of the Damara Orogon (modified from Miller, 1983) 2

Figure 3: Map of Gondwana showing the positions of the cratonic nuclei and the orogenic belts that weld the supercontinent together. SF = Sao Francisco craton, RP = Rio de la Plata craton. In the centre are the Kaoko, Gariep (coastal branch) and Damara (inland branch) belts (from Gray et al., 2008). 10

Figure 4: Schematic cross section of the Damara belt showing the different tectonostratigraphic zones contained (from Gray et al. 2008) 11

Figure 5: A regional geological map of the Navachab Gold Mine and its surroundings located in the southern Central Zone of the Damara collision belt. Note the typical characteristics of the sCZ namely; the doubly plunging dome structures with irregular intervening synforms and granitic intrusions (from Kisters, 2005). 12

Figure 6: Opening of the Khomas Sea, by continental rifting, offered deposition space for the formation of the Damara Supergroup (from Anthonissen, 2010). 13

Figure 7: A sketch representing crustal convergence of the Damara belt, with subduction towards the NW and/or N. These tectonics developed the first shallowly dipping D1 structures and lead to the intrusion of early granites into the CZ (from Anthonissen, 2010). 14

Figure 8: Collisional tectonics refolded earlier D1 recumbent folds to almost upright ENE trending D2 folds and brought about associated granite plutonism in the N of the Congo Craton, the present day CZ (from Anthonissen, 2010). 15

Figure 9: Crustal thinning and extension of the Damara belt followed collisional tectonics and are associated with the intrusion of numerous post- and late-tectonic granites. These intrusions are linked to numerous high T, low P metamorphic events occurring between 505Ma and 478Ma (from Anthonissen, 2010). 16

Figure 10: A simplified geological map of the Navachab open pit showing the main pit and contained lithological formations. The blue arrows show the plunge of the Main, Second and possible Third en-echelon ore shoots. The Spes Bona Formation, in the east, contains mineralized quartz-sulphide veins that form part of the Main Shoot ore body (Internal report by Rockwater Consulting, 2008). 27

Figure 11: A schematic diagram of the Navachab open pit looking to the NNE. The lithological formations exposed include the Spes Bona, Okawayo and Oberwasser which all dip steeply towards the WNW (to the left of the diagram). Mineralization is hosted by quartz-sulphide veins crosscutting the sub-vertical lithologies. The host rocks are intruded by numerous pegmatite, aplite and lamprophyre dykes with concordant and discordant contact relationships (from Kitt, 2008). 28

Figure 12: Lithostratigraphic column through the lithologies observed within and around the Navachab open pit (after Kitt, 2008). The red intrusions schematically represent aplite and pegmatite intrusions. 29

Figure 13: Shows a fresh rock specimen and thin sectional of the biotite schist. Note the oval biotite rings with quartz cores, the section is 1.25mm wide. 30

Figure 14: Shows a fresh rock specimen and thin section of the calc-silicate sub unit. The thin section is 0.6mm wide. 31

Figure 15, A aplite dyke in the FW sequence cross-cut by a shallowly dipping quartz vein (top) as it cross-cuts another shallowly dipping vein (bottom). This suggests the intrusion of felsic dykes swarms and quartz veins were syn-genetic. 33

Figure 16: A stereographic projection of poles to the plane bedding readings taken along the FW sequence. The S0 foliation (bedding) observed in the Navachab open pit is relatively uniform as no secondary folding (F2b) is present. 35

Figure 18: A) a plan view map showing the outline of the Navachab open pit. Red and green marks represent all selected diamond drillholes used to gather petrographical (red and green marks) and structural (green marks) data in the study. B) Is a plan view level map, modelled in Datamine, of level 1075. All holes were drilled perpendicularly into the FW sequence. C) Is a cross section of the main pit along section line 2700, looking towards the NE. The pit outline in grey with lithological contacts drawn in blue, orange and green wireframes represent ore envelopes and in red are some of the holes used for this study. 38

Figure 19: Stereographic contour plot of poles to the plane from planar vein orientations readings taken on the 10 selected holes. Note the strong bias towards the bedding parallel and S2 (axial planar) vein sets due to the horizontal drilling orientation. The black half circle defines the average dip (73˚) and dip direction (293˚) of bedding S0. 40

Figure 20: Shows a cross section, looking NNE, thru the Navachab Main Pit with the different lithologies demarcated. The three main quartz vein sets, as they occur within the Spes Bona Formation, are schematically represented along with a drill line showing the general azimuth and dip of the holes drilled for this study. From a Navachab internal report, 2008. 41

Figure 21: A) A contour plot of poles to the plane of historic vein orientation data gathered from pit mapping and vertically drilled core from the FW sequence. Note the strong bias towards the horizontally trending CVS. 42

Figure 22: A bar graph with vein set % as hosted within the FW sequence. 43

Figure 23: Ore paragenesis quartz-sulphide veins, observed under a reflective light microscope (after Wulff, 2008). 44

Figure 24: A) Represents the garnet-biotite alteration type observed in a hand specimen (right). On the left, and a comparative view from under the microscope is provided between altered and unaltered biotite schist of the FW sequence. The same was done for (b) where actinolite-quartz alteration is represented under the microscope and in a hand specimen (from a Navachab internal presentation)... 46

Figure 25: A) Shows a boudinaged bedding parallel vein with remobilised pyrrhotite concentrated in the boudins neck, the neck is 2cm across. B) Illustrates folding in a conjugate vein cross-cutting bedding at steep angles, scale is in cm. Red arrows indicate the co-axial shortening strain developed at high angles to the bedding, the regional shortening strain. 47

Figure 26: Cross-section cartoon of the Karibib Dome during regional NW-SE directed shortening. A) Represents amplification of the Karibib Dome, where flexural flow along bedding contacts developed a plumbing system for the BPV set. B) Depicts fold lock up and the development of extensional fractures sucking in over-pressurised hydrothermal fluids to form the CVS (from Kister, 2005). 48

Figure 27: A and B are pictures representing the genetic relation between the CVS and the BPV set. In (A) bedding parallel veins developed after the formation of conjugate veins and in B the different sets developed concurrently. These observations propose bedding parallel veins developing syn- to post-genetically with the conjugate vein set. Note how in A the BPV displaced the CVS and the pronounced folding of the CVS. 49

Figure 28: Represents a WNW-ESE cross-section (looking NE) through the central parts of the Navachab Open pit (in green) with the occurring ore zones in red. Note the sub-vertical and sub-horizontal ore trends present in the FW, the lower schist, (after Vollgger et al. 2012) 50

Figure 29: A sketch representing 2 one meter drill intersects containing, in A, a BPV and in B a CVS. The sketch illustrated how drilling sub-parallel to the CVS increases the volume of vein material vs. host rock material for that sample interval. A BPV of similar thickness will have a much higher vein to host rock material ration, influencing the assay result negatively. 56

Figure 30: The mineralisation model (Steven et al., 2014) explains how metamorphic dehydrated resulted in the release of fluids. Collisional tectonics further facilitated the development of primary fluid path ways transporting the enriched fluids to a deposit scale. Here hydrothermal fluids reacted with fluid sinks such as a physical throttle and/or a chemical trap, allowing gold to precipitate from solution. 64

Figure 31: Figure showing the mineral system concept for the development of ore deposits (after Hronsky et al., 2010) 69

Figure 32: Presents the scale dependant targeting criteria for most orogenic gold processes (after McCuaig et al., 2009) 70

List of Tables

Table 1: Deformation phases in the CZ as described by different authors. Dates given for deformation phases are from Miller (2008). 17

Table 2: A lithological column outlining the host rocks of the Damara belt, the Damara Supergroup (after Badenhorst (1992), modified from Kitt, 2008). 19

Table 3: Describes the geochronological relationship developed between mineralisation, igneous and tectonothermal events observed within the South Central Zone, modified from Stevens et al., (2014). . 25

Table 4: Fabric elements that can be ascribed to the main deformation phases, D1 and D2 are summarized (after Kitt 2008). 34

Table 5: the volume % of rock mineralized is compared between calc-silicate felses and biotite schist. The plotted trend highlights the schistose units as having a higher rock volume of mineralized material, thus acting as a better host to quartz vein development within the FW. 53

Table 6: shows the average grade for each sub-unit of rock according to different cut-off grades. 54

Table 7: The number of veins per set, and average grade of these are plotted. As a similar number of veins were identified for each set, the CVS appears to have the highest average grades. 55

Table 8: Grades of different veins from each vein set was assayed. The BPV and S2V returned the highest grades, almost twice that of the CVS. 57

Table 9: Shows the average grades for the 10 veins per vein set, note the high values recorded for the BPV and S2V. 57

Chapter 1: Introduction

1.1 Locality

The Navachab Gold Mine (NGM) is currently (2013) the only gold producing mine in Namibia situated about 10km southwest from the town of Karibib, some 150km southeast from Windhoek (Figure 1). Gold occurs as free gold within stratabound quartz-sulphide lenses and sets of quartz-carbonate veins.

Figure 1: Location of the Navachab Gold Mine, situated 10km SW from Karibib on the NW limb of the Karibib Dome (Google Earth).

Geologically the NGM lies within the south Central Zone of the Pan-African Damara Belt (Figure 2). This orogenic belt is a deeply eroded, late Neoprotorozoic (550-500 Ma) oblique collision suture between the Kalahari and Congo Cratons (Miller, 1983; Kasch, 1983a; Jung, 2000; Jung et al., 2002).

Host rocks comprise of a shelf- to continental slope-type sequence metamorphosed to amphibolite-facies conditions (Miller, 1983). The main economic-grade gold

mineralization is controlled by two doubly plunging anticlines, the Usakos and Karibib dome (Figure 1). The steeply dipping north-western limb of the Karibib dome hosts the Navachab Gold Mine mineralisation.

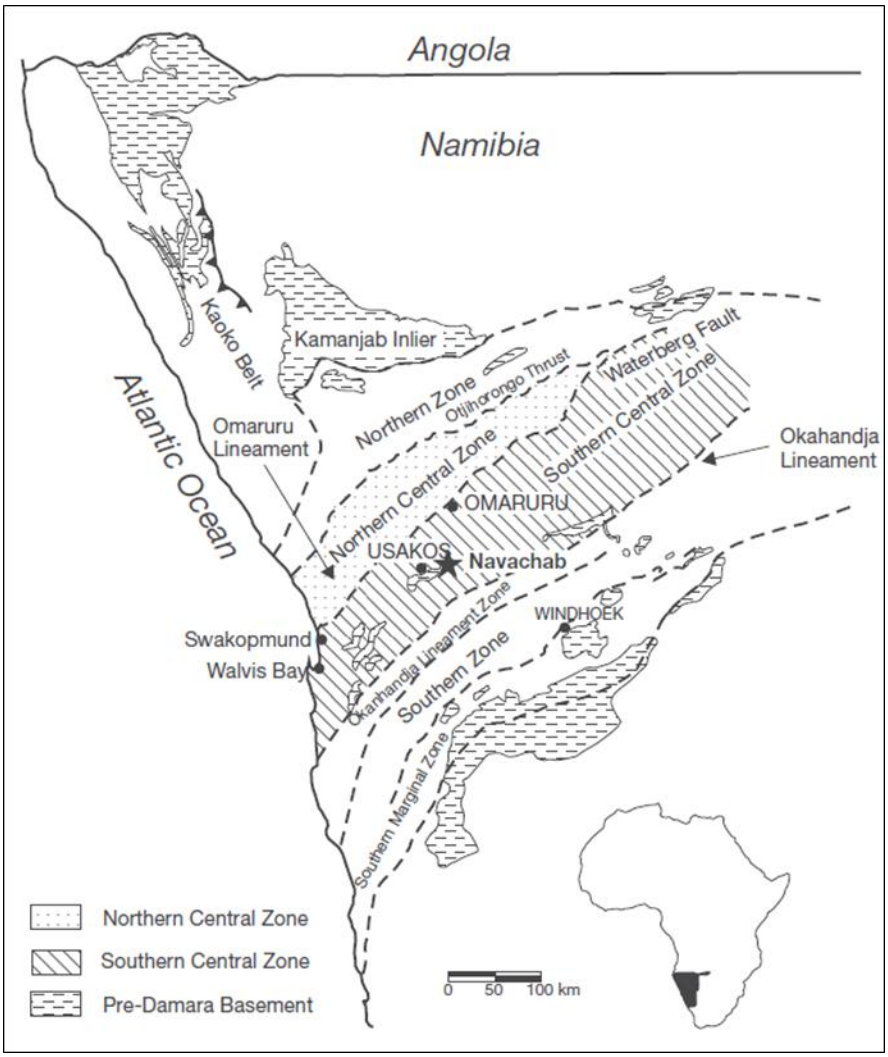

Figure 2: Location of the NGM within the main tectonostratigraphic zones of the Damara Orogon (modified from Miller, 1983)

The auriferous quartz veins, the geometry of the mineralization, its structural controls, and ore- and alteration assemblages are commonly interpreted to indicate a hydrothermal origin to the mineralization (Moore et al., 1998, 2003; Steven and Badenhorst, 2002; Kisters, 2005). Earlier genetic mineralization concepts favoured a skarn model (e.g. Pirajno and Jacob, 1991; Nortemann et al., 2000). Recent works

postulate that the swarm of sheeted quartz veins forms the main mineralizing system, which combines many characteristics of mesothermal, orogenic lode-gold deposits (Moore and Jacob, 1998; Moore et. al., 1999; Steven and Badenhorst, 2002; Kisters, 2005, Kitt., 2008). These deposits occur throughout the Earth's history where they develop in back arc, arc or accretionary prism situations throughout the later orogenic evolution stages, characterized by Cordilleran-style tectonics (Kerrich et al. 2000; Goldfarb et al., 2001; Groves et al., 1998, 2003; Kolb, 2008).

1.2 Background and Rationale

Orogenic lode-gold deposits are gold-bearing quartz- and quartz-carbonate vein systems having a hydrothermal source with a close temporal and spatial association to deformation and metamorphism during crustal convergence and collisional tectonics (Kerrich et al., 2000; Goldfarb et al., 2001). These auriferous quartz-vein systems form in the brittle-ductile regime under greenschist-facies or higher-grade metamorphic conditions. Here, crustal depths allow for very low rock permeabilities and fluid transport is controlled by fracture development (Sibson, 1996, 2001; Sibson and Scott, 1998). Vein systems thus form in regional-scale and associated second and third- order structures (e.g. Sibson et al.,1988; Hodgson, 1989; Cox et al., 1991, 1995; Ridley, 1993; Groves et al., 1998, 2003; Kerrich et. al. 2000; Robert and Paulsen, 2001).

The behaviour and formation of the paleoplumbing system, bringing about the mineralization, is commonly, although not exclusively, country-rock rheology controlled, especially at prominent lithilogical contacts (Groves et al., 1998, 2003; Kerrich et al., 2000; Stevens et al., 2003; Kisters., 2005; Kitt., 2008). A number of different fluid origins

are discussed for lode-gold deposits including metamorphic, meteoric and/or magmatic fluids (Sibson and Scott, 1998). These source fluids are lithostatically over pressurized in order to infiltrate low displacement faults or shears which are connected by hydraulic extension fractures, resulting in large-scale fluid throughput of the otherwise largely impermeable high-grade metamorphic wall rocks (Etheridge et al., 1983; Hodgson, 1989; Cox et al., 1991; Sibson, 1996, 2001; Sibson and Scott, 1998). Gold and sulphides transported by the circulating hydrothermal fluids would precipitate as a result of fracturing and abrupt P-T variations in and around veins, changing Eh-Ph conditions as a result of phase separation in the hydrothermal fluid, or, for example, sulphidation reactions around ferruginous wall rocks, to name just some of the more important processes.

The NGM mineralization is confined by two main quartz-vein geometries, namely:

a) high grade stratabound quartz-sulphide lenses (plunging shallowly towards the NE, parallel to the fold axis of the Karibib dome) found at the base of the marble-dominated Okawayo Formation along the contact with the underlying, siliciclastic Spes Bona Formation, and

b) a medium grade discordant, sheeted quartz-vein system that cuts through several formations of the Damara Supergroup (Moore et al. 1998, Steven and Badenhorst 2002; Kisters 2005; Wulff, 2008; Kitt, 2008).

This study focusses on the distribution of mineralization within the Spes Bona Formation, locally known as the Footwall unit.

1.3 Aims of the study

The geometry and structural inventory of hydrothermal vein systems and associated fluid plumbing systems of orogenic gold deposits is substantial help in unravelling the evolutionary path of hydrothermal vein systems and lode-gold deposits (e.g. Windh, 1995; Ridley and Mengler, 2000; Robert and Poulsen, 2001; Schaubs and Wilson, 2002). The structural setting of the Navachab hydrothermal vein system has, by past and recent works, been investigated in great depth and a good understanding of the associated veins and their development, individual vein sets and their orientations, and controls to the mineralization have since been reached.

This present study is focused on the Footwall section (Spes Bona Fm) of the Navachab deposit where ore (gold-bearing grade) envelopes are of an irregular and scattered nature. The Footwall (FW) sequence plays host to about 60% of the total Navachab resource of 3.7 Moz gold at a 0.4 g/t cut-off grade of gold. With no other ore scheduled for mining within the next 3 to 4 years, the importance of the FW ore as primary plant feed becomes apparent.

By combining historic knowledge (structural setting, vein and vein set formation) with local observation, this study aims to identify and measure factors impacting on ore formation and distribution throughout the Footwall Spes Bona Formation. These factors will establish the main controls defining ore bodies, thus establishing search ellipsoid parameters for optimal resource modelling of the ore bodies.

The main factors under investigation are summarized as follows, along with individual aims and their expected outcomes:

a) Different sub-units within the FW lithology and their degree of mineralization. The need exists to understand the local lithological control of different sub-units of the FW sequence, which hosts the gold mineralization. The aim is to identify the host rocks most susceptible to vein development of an economic gold grade. This again will help in determining optimal drill and resource modelling orientations.

b) Quartz vein sets and their degree of mineralization. The aim is to relate each vein set to grade in order to determine its importance to the FW mineralization. This will add value in determining optimal drill and resource modelling (search ellipsoid parameters) orientations.

c) Ore displacement by regional and local faulting and shearing. Displacement in the FW sequence is commonly observed within the pit and in diamond drill core. The study will additionally aim to quantify the scale and orientation of the displacement and the effect thereof on the distribution of ore in the FW.

d) All the above mentioned factors will be taken into account in order to develop a Footwall ore model. The model aims to:

- Explain how and where gold develops, and what influences the (re)distribution of gold thereof within the FW.
- Add guidance for optimal decision making regarding target generation, drill plan development, resource modelling, grade controlling and mining method applied to the current FW reserves and resources.
- Guide Exploration Geologist in locating other, similar deposits within the Damara Belt’s south Central Zone.

1.4 Methodology

The FW ore body was modelled by wireframing ore envelopes using CAE Datamine Studio 3 and Leapfrog software. Wireframes are drawn around diamond drill holes intersecting mineralized material and applied to developing a block model. The resulting model is interpreted to indicate ore distributed throughout the FW rock sequence.

Structural and petrographic investigations of the FW host rocks and different vein sets contained were completed on 39 weep holes (WH). Holes were selected to cover the FW sequence along, and across strike. Weep holes are diamond drill holes drilled perpendicularly into the pit wall (the FW sequence) for dewatering purposes. These holes were selected as the preferred study material as previous structural and petrographic investigations on the FW were done within the open pit, or on near vertical drill holes into the host rocks. This provided a bias observation view of the sub-horizontal ore distributions, negatively affecting exposure of the sub-vertical ore trend. Drilling perpendicularly into the FW offers a cross-sectional look into the sequence, emphasizing the sub vertical ore controls.

The WH's were geologically logged, gathering information on different FW sub-units, their position, thickness, contained quartz veins (grade) and observed displacement (faulting).

Over 1500 quartz veins were structurally measured by using a core orientating rig to orientate the drill core and a Breithaupt structural compass. These measurements were plotted on stereonets, all projections are equal area projections into the lower hemisphere. All planar fabrics are given as dip and dip direction and all linear fabrics are given as plunge and plunge direction. The alteration type, host rock type and

thickness of the veins were recorded as these parameters are considered to have an influence on the Au grade and distribution within the FW host rocks. The gathered information is interpreted to identify certain quartz vein sets into which each vein is classified.

Holes are sampled on one meter intervals, related to host rock type, and analysed for gold at the Burea Veritas Laboratories located in Swakopmund, Namibia. All samples were prepared by drying, crushing and milling, by a vibrating pulveriser, them to the specific sample size fraction. The samples were analysed by fire assay to give the total separation of gold. Gold concentrations were determined by Inductively Coupled Plasma Optical Emission Spectronomy (ICP-OES)

Assay results were subjected to AngloGold Ashanti's high quality assurance/quality control (QA/QC) standards to ensure reliable results were obtained.

Results of the above mentioned investigations are interpreted with the purpose of developing a Footwall ore formation and distribution model by:

a) Comparing grade results to different host rocks and contained vein set(s). The comparison will help identify the sub-unit most susceptible to quartz vein (grade) development and, which vein set(s) carries the most prolific grade, i.e. is the most important in bringing about a mineable ore reserve.

b) Displacement (faulting/shearing) observed in core is to be interpreted and if feasible related to large scale fault models, likely causing the redistribution of ore bodies within the Footwall.

Chapter 2: Regional Geology

2.1 Introduction

The Damara orogen in central Namibia forms part of the larger Pan African collisional belts, cutting into and surrounding the African continent (Porada, 1989). The orogeny formed during the amalgamation of the Gondwana supercontinent during the late Proterozoic and early Phanerozoic (Miller, 1983; Prave, 1996; Trompette, R., 2000 & 1997; Gray et al., 2008).

Collision of the Congo and Kalahari Cratons resulted in the formation of the Damara belt (Figure 3) and is known as the “intracratonic” or “inland” branch of the Damara orogeny. The N-S trending “coastal-branches” of the orogeny are made up of the Kaoko and Gariep belts which record the collision between the African cratons and the Sao Francisco and Rio de la Plata cratons of South America (Gray et al., 2008). Collisional tectonics in the Damara orogen commenced with the closure of the Adamastor Ocean between the Congo and Kalahari cratons, and the Rio de la Plata craton resulting in the formation of the Kaoko belt. Closure of the southern Adamastor Ocean followed to form the Gariep belt. Closing of the Khomas Ocean between the Kalahari and Congo cratons resulted in the Damara belt, thus concluding the orogeny.

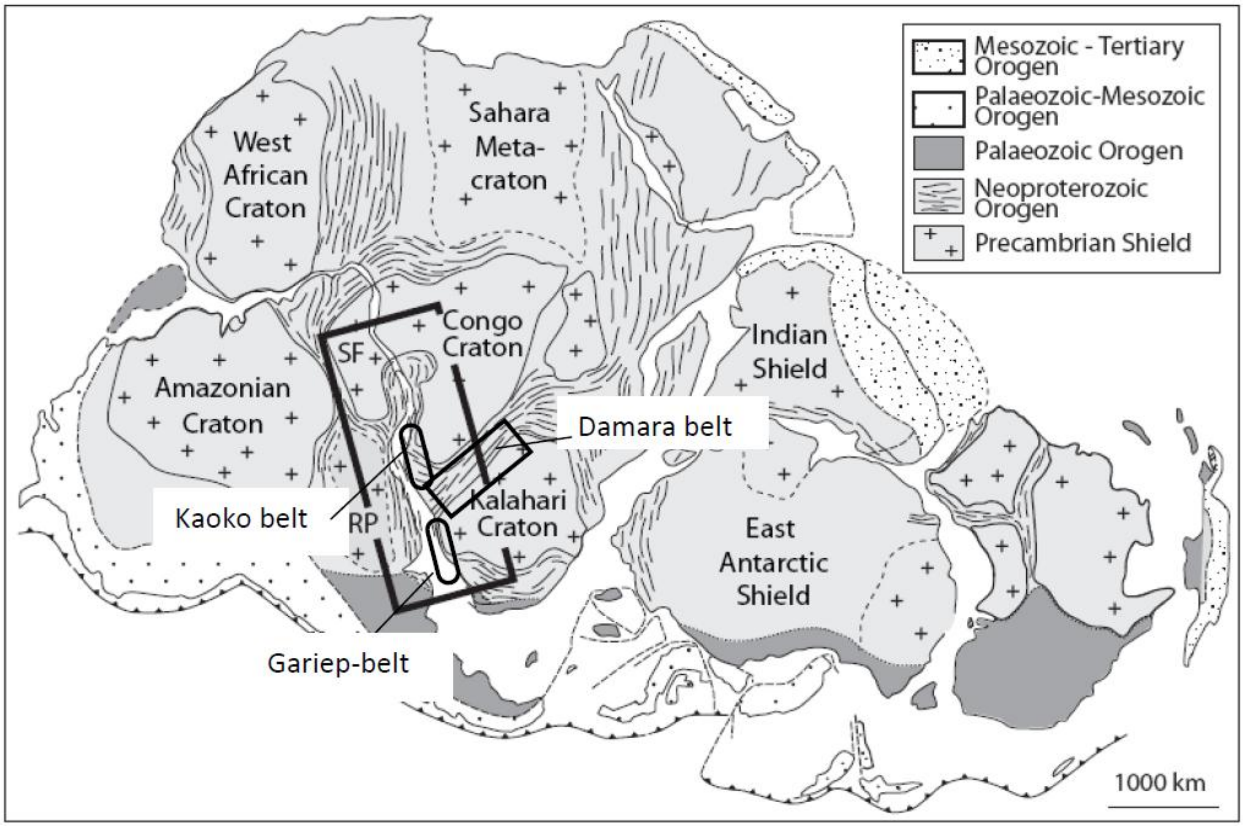

Figure 3: Map of Gondwana showing the positions of the cratonic nuclei and the orogenic belts that weld the supercontinent together. SF = Sao Francisco craton, RP = Rio de la Plata craton. In the centre are the Kaoko, Gariep (coastal branch) and Damara (inland branch) belts (from Gray et al., 2008).

The Damara belt extends close to a 1000km along an ENE trend with a width of about 400km (Miller, 1983). It consists of pre-collisional Paleoproterozoic (ca.2.0-1.7Ga) basement rocks overlain by Neoproterozoic (ca. 800-550 Ma) Damara Supergroup rocks all intruded by a large number of convergent, collisional and post-collision related granitic events (Miller, 1983, Porada, 1989; Jung et al., 1999; Gray et al. 2008).

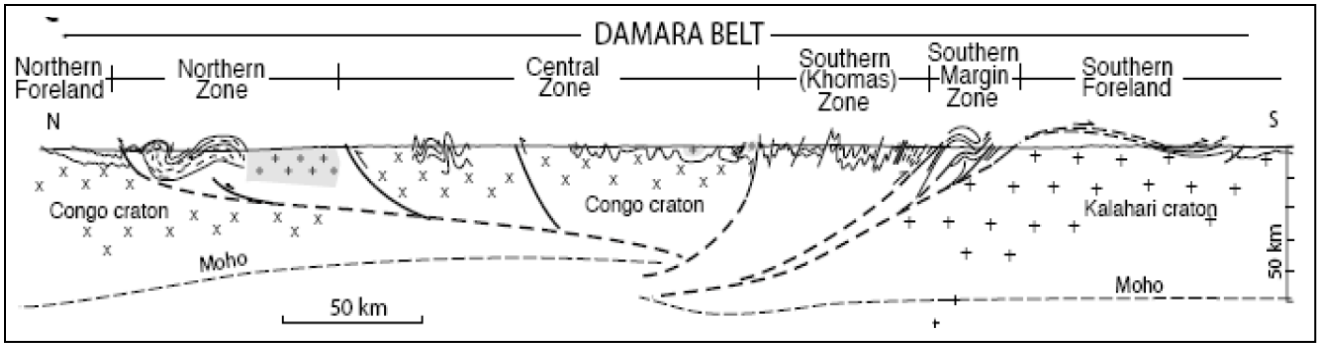

Figure 4: Schematic cross section of the Damara belt showing the different tectonostratigraphic zones contained (from Gray et al. 2008)

The collision belt is sub-divided into distinct tectonostratigraphic zones due to variations in metamorphic grade, stratigraphy, aeromagnetic signature, magmatism, geochronology and deformation observed for each zone (Martin, 1965; Martin & Porada, 1977; Barnes & Sawyer, 1980; Miller & Hoffman, 1981; Miller, 1983; Corner, 1983, 2000; Anderson & Nash, 1997). These zones (Figure 4) are as follows, from south to north; the Southern Foreland (SF), the Southern Marginal Zone (SMZ), the Southern Zone (SZ), the Central Zone (CZ) is divided into a southern (sCZ) and northern Central Zone (nCZ), Northern Zone (NZ) and the Northern Platform (NP).

The Navachab Gold Mine lies within the magmatic arc of the belt known as the south Central Zone (sCZ). The zone is characterized by regional-scale NE-SW trending doubly-plunging anticlines (e.g. the Karibib and Usakos dome structures), more irregularly-shaped intervening synforms with a variety of syn-, late-, and post-tectonic granites intruding the terrain between ca. 565 and 465 Ma, Figure 5 (Hoffman, 1976; Blaxland et al. 1979; Miller, 1983, 2008; Hawkesworth & Marlow, 1983; Tack & Bowden, 1999; Jung & Mezger, 2003).

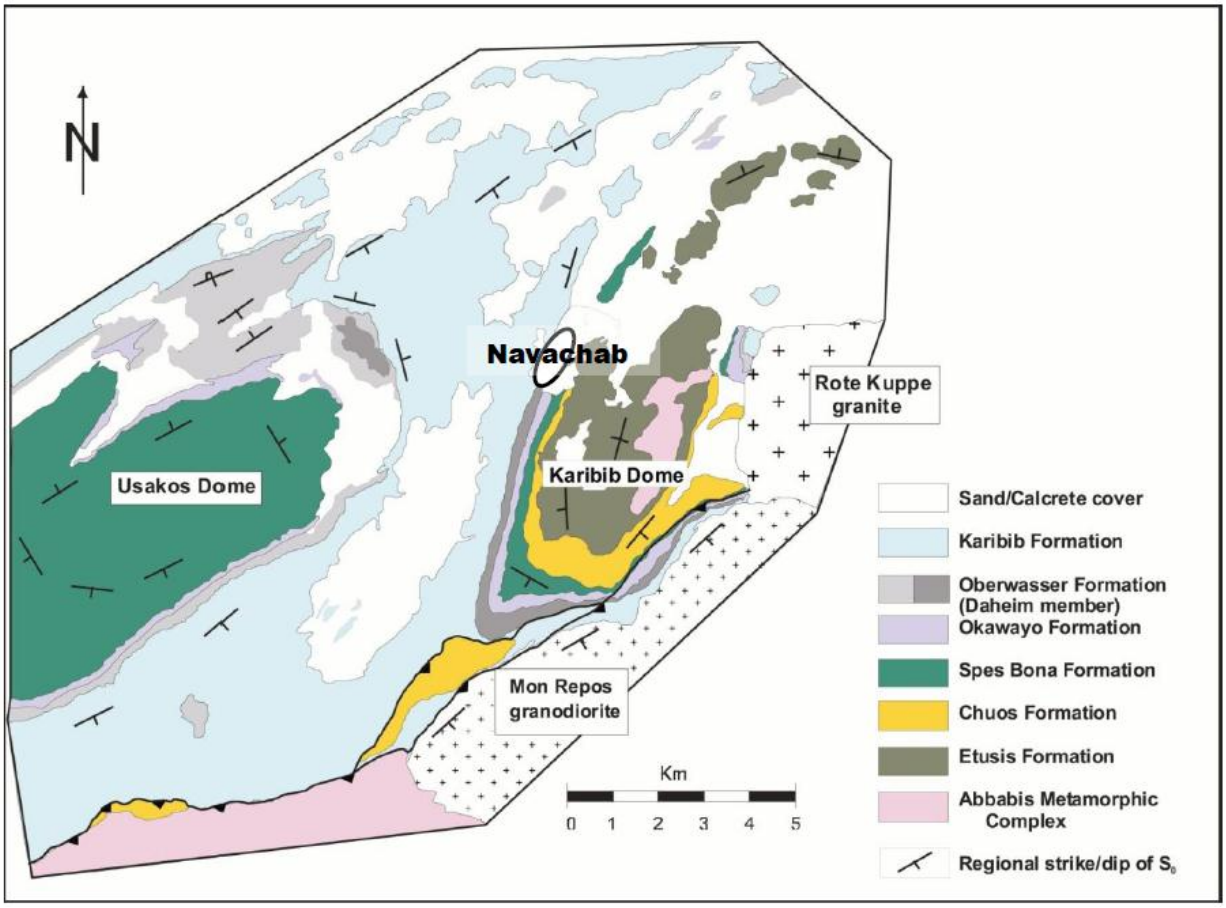

Figure 5: A regional geological map of the Navachab Gold Mine and its surroundings located in the southern Central Zone of the Damara collision belt. Note the typical characteristics of the sCZ namely; the doubly plunging dome structures with irregular intervening synforms and granitic intrusions (from Kisters, 2005).

Kilometer-thick meta-turbidite sequences make up the Southern Zone, representing the accretionary prism of the Damara belt. The prism rests on the underthrusted slab of the Kalahari Craton (Kukla & Stanistreet, 1991; Stanistreet et al. 1991; Kasch, 1983a). The Matchless Amphibolite Belt supports the accretionary prism concept as it's interpreted to represent an ophiolite sliver (Kukla & Stanistreet, 1991). The Southern Marginal Zone (SMZ) and the Northern Zone (NZ) signify the fold-and-thrust belts of the collision suture, verging SE and NW respectively (Figure 4). The belt's foreland basin is embodied in the north by the Northern Platform and in the south by the Southern Foreland.

2.2 Evolution of the Damara Belt

As this section only provides a summary of the evolution of the Damara orogen, more detailed accounts can be found in Anthonissen (2010), Miller (1983), Porada (1989), Stanistreet et al. (1991) and Gray et al. (2008).

Continental rifting along a triple junction between the Congo, Kalahari and Rio de la Plata Cratons (Miller, 1983; Porada, 1989) was already in progress by ~750Ma and lead to the deposition of the Damara Supergroup (Figure 6). Basal continental sediments and volcanic rocks of the Nosib Group (Central Zone) were unconformably deposited on Mesoproterozoic, ca. 1.8-2.0 Ga gneisses of the Congo Craton (Jacob et al., 1983). Long-lasting rifting led to the development of marine sedimentation in deep water basins which continued until ca. 580-600 Ma when the Khomas sea closed up due to crustal convergence between the Congo and Kalahari Cratons (Gray et al., 2006).

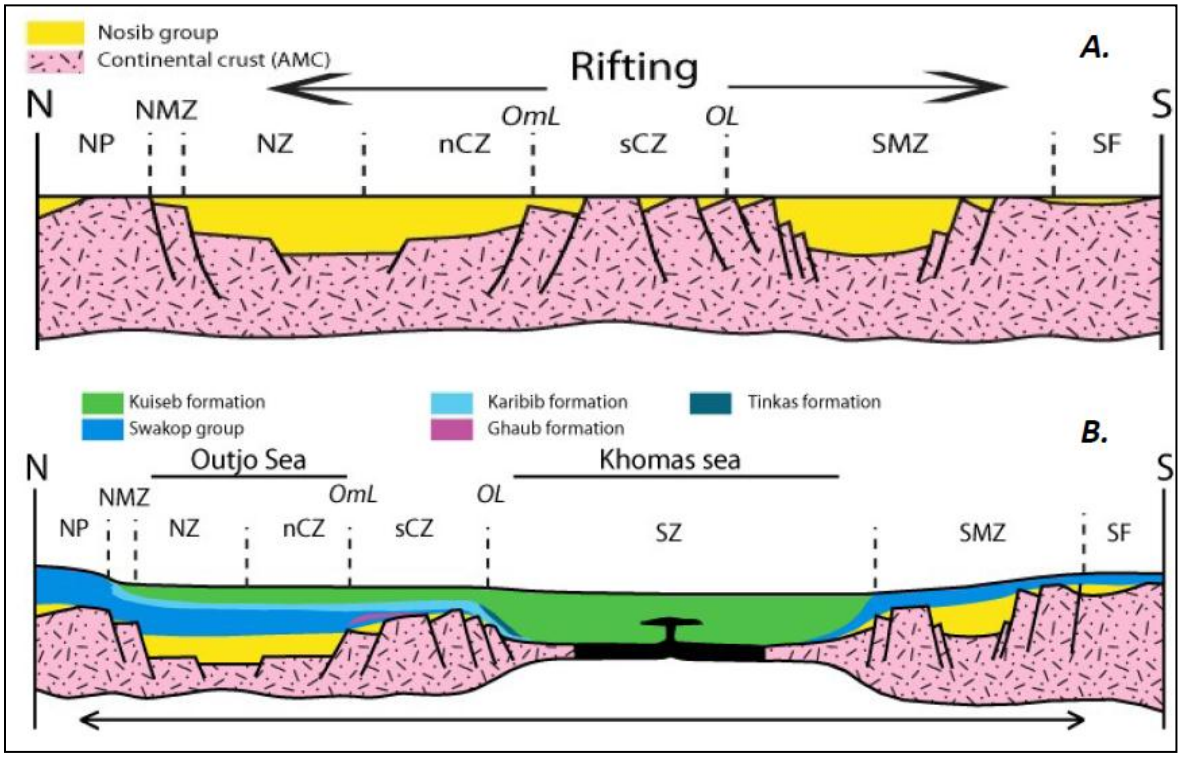

Figure 6: Opening of the Khomas Sea, by continental rifting, offered deposition space for the formation of the Damara Supergroup (from Anthonissen, 2010).

The Damara belt converged due to the N-ward subduction of the Kalahari craton underneath the Congo craton (Figure 7), Miller, 1983. Shallow to deep-marine turbidite and carbonate sedimentation dominated along the southern margin of the Congo Craton, depositing the Swakop Group (a mixed carbonate-siliciclastic succession) within the CZ.

The Kalahari Craton continued to be a major source of siliciclastic sediments, forming a thick repetitive turbidite sequence that makes out the accretionary prism deposits lying above the down going plate of the Kalahari Craton (Stanistreet et al., 1991).

The development of a regional bedding-parallel (S1) fabric, and large-scale thrusting and recumbent folding (D1, Miller, 1983) is associated with crustal convergence between ca. 580-550Ma. The period also saw numerous small gabbroic, dioritic and syenitic plutons intruding throughout the central Damara belt (Jacob et al., 2000; de Kock., 2000).

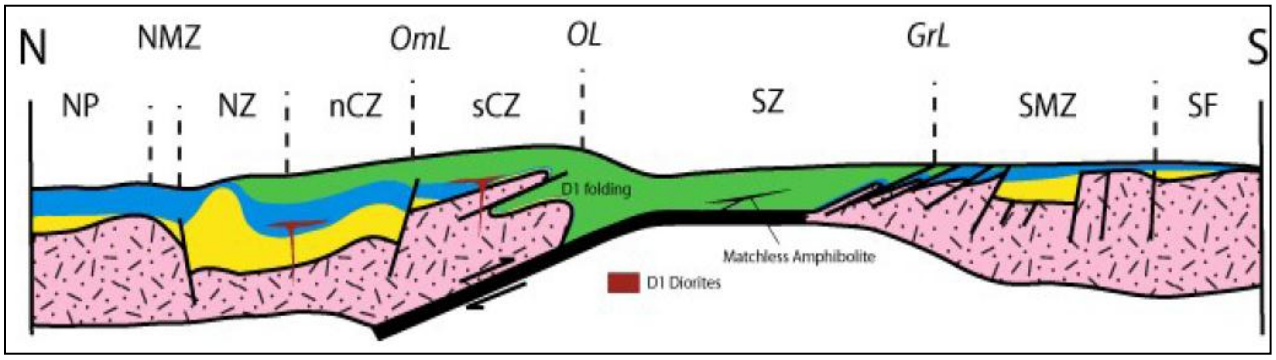

Figure 7: A sketch representing crustal convergence of the Damara belt, with subduction towards the NW and/or N. These tectonics developed the first shallowly dipping D1 structures and lead to the intrusion of early granites into the CZ (from Anthonissen, 2010).

The ensuing high-angle collision event (550-540Ma) between the Cango and Kalahari Cratons gave rise to the main regional NE trending structural grain (Figure 3 & Figure 5) observed throughout the Central Zone (Miller, 1983; Gray et al., 2006). Development of regional-scale fold-and-thrust tectonics, regional-scale dome structures with associated

intervening synclines (D2) and the intrusion of widespread syntectonic granites (Figure 8) also resulted from the colission tectonics (Miller, 1983; Jung et al., 2001; Johnson et al., 2006).

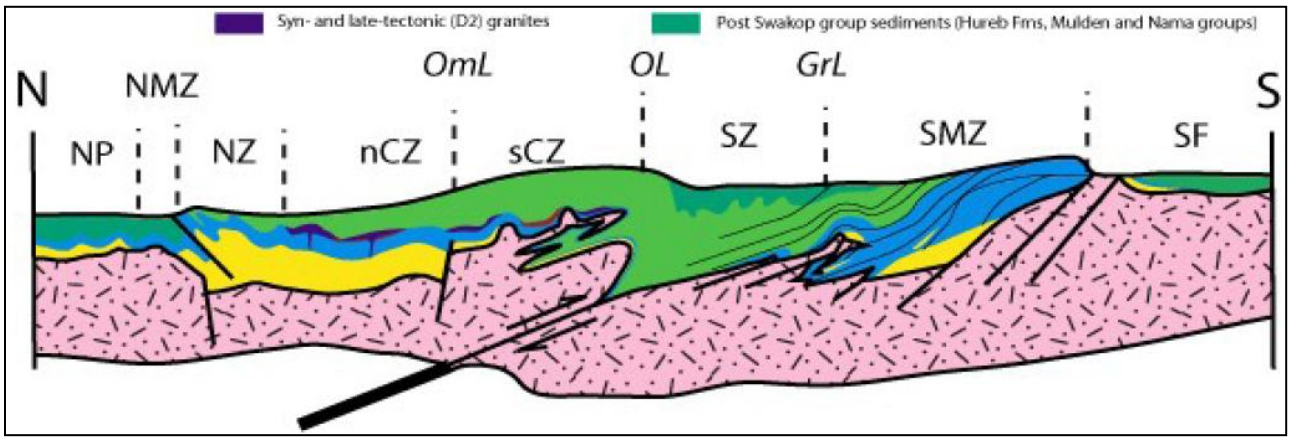

Figure 8: Collisional tectonics refolded earlier D1 recumbent folds to almost upright ENE trending D2 folds and brought about associated granite plutonism in the N of the Congo Craton, the present day CZ (from Anthonissen, 2010).

Crustal thinning and extension followed collision due to the uplift and decompression of the Damara belt rocks, Figure 9, (Tack and Bowden, 1999; Jung and Mezger, 2003; Johnson, 2006). The post-collision evolution also entailed the intrusion of numerous post- and late-tectonic granites between 540-480 Ma (Hoffman, 1976; Jacob et al., 2000; Jung & Mezger, 2003). This final stage of granitic plutonism is associated with a high-temperature, low-pressure metamorphic event responsible for the current metamorphic assemblages observed for the sCZ. The metamorphic event reached numerous peaks between 505Ma and 478Ma (Bowden et al., 1999; Jacob et al., 2000; Jung & Mezger, 2003). Final uplift of the central parts of the Damara belt was established by Ar-Ar cooling ages to have occurred at ca. 460(Gray et al., 2006).

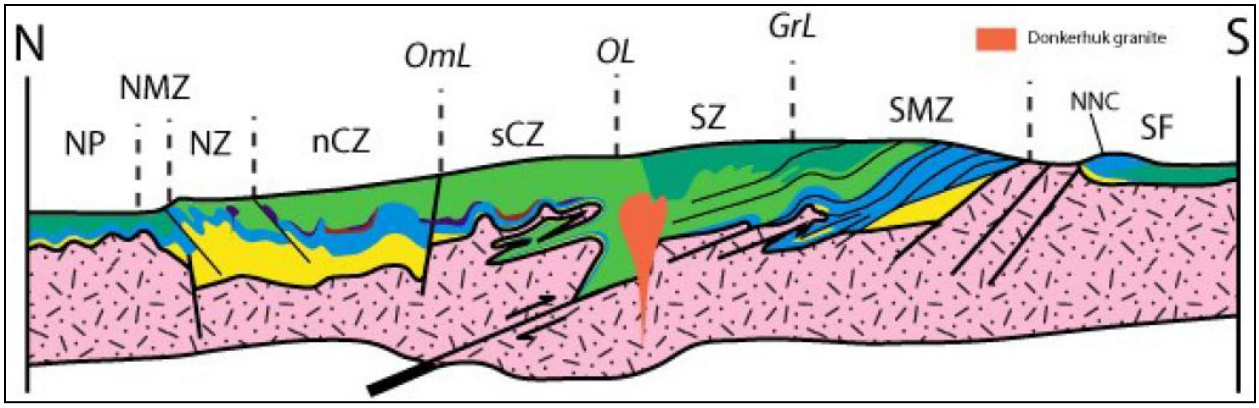

Figure 9: Crustal thinning and extension of the Damara belt followed collisional tectonics and are associated with the intrusion of numerous post- and late-tectonic granites. These intrusions are linked to numerous high T, low P metamorphic events occurring between 505Ma and 478Ma (from Anthonissen, 2010).

2.3 Structural Setting of the sCZ

Structural investigations into the sCZ show evidence for a polyphase deformation history (Miller, 2008). Most works describe 3 main deformation phases, D1 to D3, with some authors such as Jacob (1974) Barnes & Sawyer (1980), Sawyer (1981), De Kock (1989) and Steven (1993) adding a D4 phase (Table 1).

Recent studies support only 2 main deformation phases (D1 and D2), where earlier D3 and D4 features are interpreted as the result of an extended progressive D2 phase, see Oliver (1994), Poli & Oliver (2001), Kisters et al. (2004) and Johnson (2006).This study, following Poli and Oliver (2001), ascribes deformation observed across the Damara Belt to two progressive events, namely D1 and D2:

D1 is associated with continental convergence that eventually led to the development of shallow thrusts, recumbent folds and the associated shallow S1 cleavages forming parallel to bedding (S0). D2 is responsible for reworking and refolding earlier D1 features, this D2 overprint makes identifying D1 structures almost impossible.

Deformation phase	Jacob (1974)	Sawyer (1981)	Steven (1993)	Poli & Oliver (2001)	Kisters et al. (2004)	Miller, (1983; 2008)	Age of deformation
D1	**D1** - S1 is axial planar to mesoscopic isoclinal F1 folds. F1 folds refolded by later deformation.	**D1** - Tight to isoclinal folds with sub-horizontal axial planes.	**D1** - S1 is a bedding (S0) parallel fabric often seen wrapping around domes	**D1** -A strong S1-fabric is defined by biotite and quartz alighnment parallel to S0. L1 fabrics are formed by sillimanite, cordierite and feldspar.	**D1** - A Bedding parallel/sub-parallel foliation and associated F1 intrafolial folds. Low angle thrusting and truncation faults	**D1** - Local D1 thrusts and large scale F1 recumbent folds	Prior to 560 Ma
D2 (Early D2)	**D2** - F2 defines the NE structural trend for many areas in the CZ, forming large scale antiforms and synforms. Folds can be isolclinal, but fold tightness is a function of variable rheology.	**D2** - A S2 fabric defined by biotite preferred orientation - orientated: 310-350/15-30	**D2** - Upright tight F2 folds trending 058°			**D2** - F2 sheath folds and a associated NE plunging L2 mineral stretching lineation	± 550 Ma
D3 (Late D2)	**D3** - Minor F3 open folds on steep F2 limbs (Scarce). A S3 fanning cleavage is occasionally developed.	**D3** - Subvertical F3 folds and associated schistosity trending 60°-240°	**D3** - Large scale upright open folds, forming F3 antiforms and synforms and a associated S3 schistosity.	**D2** - S2 planar-axial foliations are sporadically developed with no preferred orientation. Constrictional folding : sheath folds verging SW.	**D2** - Refolding of S1/S0 around domes (F2 folding) and a N-NE trending axial-planar S2 foliation. Local development of SW vergent sheath folds (D2b).	**D3** - NE trending doubly plunging domes defining the structure grain of the SCZ	< 542 Ma
D4 (Late D2)	**D4** - F4 structures are superimposed on F2 folds. F4 seen as NNE trending crenulations (scarce).	**D4** - F4 folds dipping 327/42 and plunging 45/07	**D4** - NW-verging F4 folds (late-tectonic) as well as the development of a spaced axial planar S4 cleavage. F3 seems to be rotated by F4				

Table 1: Deformation phases in the CZ as described by different authors. Dates given for deformation phases are from Miller (2008).

D2 led to the development of open to isoclinal NW-verging folds and the associated axial planar S2 cleavage observed within the Damara Belt (Anthonissen, 2010). A L2 fabric, associated with the S2 cleavage, developed with interference between F1 and F2 folds (Smith, 1965). The L2 fabric is identified by preferred mineral orientations and mineral stretching lineations plunging to the NE across the CZ (Smith, 1965; Downing & Coward 1981; Miller, 1983; Poli & Oliver, 2001).

The km-scale NE-SW trending oval dome shaped structures, characteristic of the CZ, relate to a late-D2 (D3 after Miller, 1983) event. Their formation isn't fully understood but

mechanisms have been proposed by the following authors, e.g. Smith (1965), Barnes & Sawyer (1980) Jacob (1983), Miller (1983), De Kock (1989) and Sawyer (1981), Steven (1993) and Johnson (2005).The structural setting of the sCZ changes from a granulite-facies dominated SW portion associated with SW extruded sheath folds, to more brittle deformation structures (thrust imbrications) in the NE (Anthonissen, 2010).

2.4 Metamorphism

Metamorphic conditions in parts of the southern Central Zone reached granulite-facies conditions, but amphibolite-facies grades are regionally widespread. In general, there is a decrease in metamorphic grade from SW to NE (Masberg et. al., 1992, 2000, Steven 1993; Nex et al. 2001; Jung and Mezger, 2003) as an erosional feature exposes deeper crustal parts of the belt towards the atlantic seaboard.

Peak metamorphic conditions were reached by 535-470 Ma in the SCZ (Jung et al., 2001; Jung & Mezger, 2003). Metamorphic conditions around Karibib and Usakos have been estimated to be T= 550-600°C at P= 3±1kbar (Puhan, 1983; Steven, 1993; Masberg, 2000; Jung & Mezger, 2003; Ward et al., 2008), characterizing the distinctly high-T low-P nature of metamorphism associated with the CZ. The lower amphibolite-facies metamorphic conditions led to the development of biotite-cordierite assemblages within metapelites and, clinopyroxene-actinolite-plagioclase assemblages in calc-silicate felses. Peak metamorphism recrystalized marble units where the calcite-dolomite assemblages undergone an annealing effect. Garnet only occurs in the alteration zones of rock units associated with hydrothermal quartz veining, but is regionally absent in unaltered rocks.

2.5 Lithostratigraphy

The Navachab open pit lies within the Neoproterozoic Damara Supergroup (Miller, 1983). This study follows the stratigraphy outlined by Badenhorst (1992) , shown here as a simplified lithostratigraphic column (Table 2). Mineralization is developed in rock units of the Karibib-, Oberwasser-, Okawayo- and Spes Bona Formations.

2.5.1 Abbabis Metamorphic Complex (AMC)

The AMC constitutes the oldest rocks in the area with U-Pb Zircon dating yielding ages of 1925Ma ± 330 Ma (Jacob et al., 1978). These pre-Damaran inliers represent parts of the leading edge of the Congo Craton onto which the Damara Supergroup is deposited. The basement complex consists of red, homogeneos quartzo-feldspathic augen gneisses, biotite schists, quartzites, amphibolites, intrusive pegmatites and granites and calc-silicate rocks (Miller, 1983; Brandt, 1985; Steven, 1993; Kisters et al., 2004).

	Group	Formation	Lithology
Damara Supergroup	Swakop	Kuiseb	Biotite-muscovite-cordierite schist, Metaturbidites, Metapsammites + interlayered biotite schist, quartzofeldspathic schist.
		Karibib	A massive grey and white dolomitic- and calcitic marble unit with intercalated brecciated marble- and fine calc-silicates layers.
		Daheim Member	Mafic metavolcanics (amphibolites).
		Oberwasser	Biotite-cordierite and biotite schist, minor brecciated marble layers, minor metavolcanics and calc-silicate felses. 635.5+-1.2 Ma (Hoffmann, 2004)
		Okawayo	Grey banded marbles, interlayerd calcitic marble and calc-silicate unit, brecciated marble unit, amphibolite sills and dykes, gossanous pods.
		Spes Bona	Biotite-quartz+-cordierite+-actinolite schists, meta-psammites, calc-silicate felses and minor marbles, metavolcanics and quartzites.
		Chuos	Glaciomarine diamictite, banded iron formation. 746+-2 Ma (Hoffmann et. al., 1996)
	Nosib	Etusis	Arkoses,feldspathic quartzites, conglomerates and minor pyroclastics
	Unconformity		
	Abbabis Metamorphic Complex	Augan gneiss, mylonitic gneiss, pegmatites, granite gneiss with minor hornblende gneiss and schist. 1862+-21 Ma (Becker et al., 2006)	

Table 2: A lithological column outlining the host rocks of the Damara belt, the Damara Supergroup (after Badenhorst (1992), modified from Kitt, 2008).

2.5.2 Nosib Group

2.5.2.1 Etusis Formation

The lowermost formation of the Damara Supergroup unconformably overlies the AMC (Brandt, 1985 and 1987; Steven, 1993; De Kock, 2001). The Etusis rift-type succession was derived by weathering the granitic basement about 770-760Ma ago (Miller, 1983; Hoffman et al., 1996). The Etusis Formation consists of predominantly quartzo-felspathic meta-arkoses and feldspathic quartzites with minor inter-bedded metavolcanics, calc-silicate felses, mica schists and grits (Badenhorst, 1992; Kisters et al., 2004). The Formation preserves primary sedimentary structures well, as cross bedding is commonly observed. The mainly coarse-clastic rocks formed within half-graben structures (Stanistreet et al., 1991; Henry, 1992; Miller, 2008), in fluvio-deltaic to aeolian environment and may reach thicknesses of up to 1500m in areas around the NGM (Kisters et al., 2004).

2.5.3 Swakop Group

Overlying the continental rift-type sediments of the Nosib Group is the marine, shelf- to continental slope type depositional sequence known as the Swakop Group, Table 1, (Smith, 1965; Jacob, 1974; Stanistreet et al., 1991; Henry, 1992; De Kock, 2001). The Swakop Group can reach several thousand meters in thickness in some areas of the Damara belt, but tends to thin off dramatically within the sCZ as a result of the zone's paleohigh in the Neoproterozoic (Miller, 2008).

2.5.3.1 Chuos Formation

The overlying diamictite, Sturtian-age (ca. 740Ma), Chuos Formation is a matrix-supported glaciogenic mixtite (Hoffman et al., 1996 and Badenhorst, 1992). The Formation consists of varying quartz, granite, pebbly schist, marls, marbles and

pegmatite clasts set within a greenish calc-silicate bearing schist matrix (Badenhorst, 1987). According to Kisters et al., 2004 the Chuos observed within the Karibib Dome reaches a thickness of between 80-180m.

2.5.3.2 Spes Bona Formation

The Spes Bona Formation is a meta-pelitic succession consisting of calc-silicate felses, biotite+-cordierite schists and finely laminated biotite schist with minor interbedded amphibolite, metapsammite and marble units. The interlayering of the metapelitic and metapsammitic units suggests a turbidite-like origin for the sequence. The Spes Bona Formation also shows preserved primary sedimentation features such as ripple marks and cross beds. The thickness of the formation is not well constrained and varies considerably depending on the area it's being observed at. In the main pit of the NGM, the formation is ca. 150-200m thick, on the SE limb of the Karibib dome the Spes Bona Formation is less than 20m thick, whereas in the Usakos dome it is thicker than 600m. The varying thickness over relatively short lateral distances is explained by Kisters et al., 2004 to be the result of a structural elimination (faulting) occuring at the boundaries of the formation.

2.5.3.3 Okawayo Formation

The calcitic and dolomitic marbles and intercalated calc-silicate felses of the Okawayo Formation, overlying the Spes Bona Formation, consists of two parts. The lower part (host to the high grade massive sulphide lenses) is an intercalated calc-silicate fels and calcitic marble sequence, with a calc-silicate fels free dolomitic upper part. The calcitic marbles are grey-bluish to white in colour, while the dolomitic marbles have creamish weathered surfaces and are white-grey when freshly struck. The marbles occur as massive and/or banded and/or intercalated sedimentary marble breccias units within the

Okawayo Formation. Calc-silicate felses tend to be brown-reddish when weathered and greenish-grey when fresh. Calc-silicate layers vary from 1 to up to 10cm in thickness. In the Karibib Dome the Okawayo Formation is about 80m, whereas it reaches a thickness of up to 150m in the Usakos Dome (Kisters et al., 2004; Steven, 1993).

2.5.3.4 Oberwasser Formation

The overlying Oberwasser Formation is very similar in composition to the Spes Bona Formation. It forms the hangingwall ore body in the Navachab main pit. According to Hoffmann et al. (2004) the upper parts of the Oberwasser Formation has a glacio-marine origin having formed during the Marinoan-type glaciations (Hoffmann et al., 2004; Miller, 2008). The 60 to 160m thick succession consists of calc-silicate felses, biotite-cordierite schists, a banded siliciclastic sequence of dark grey biotite schists, minor carbonate breccia horizons and interbedded amphibolites (mafic volcanics) of the Daheim Member (Badenhorst, 1992). Hoffmann et al. (2004) used U-Pb zircon dating of ash layers in the sequence to constrain the age of sedimentation at 635.5 ± 1.2Ma.

2.5.3.5 Karibib Formation

The Karibib Formation is a calcitic and dolomitic marble unit of at least 500m thickness (Badenhorst, 1992; Kisters et al., 2004). Structural duplication may however lead to thicknesses of well over 1.2km (Johnson et al., 2006, Kitt, 2008). Dark-grey marbles are the result of very fine-grained graphite in the marble units. Finely banded, intercalated calc-silicate felses and meter-thick sedimentary marble breccia layers also occur throughout the sequence (Badenhorst, 1992; Steven, 1993). Competence contrasts between the calc-silicate and marble units develop impressive boudinage and/or folding structures.

2.5.3.6 Kuiseb Formation

The Kuiseb Formation is the upper-most unit within the Damara Supergroup. The more than 1000m thick unit contains quartz-biotite-muscovite schists, metapsammites, biotite schists and biotite schist±cordierite intercalated with calc-silicate layers (Badenhorst, 1992; Steven, 1993). Very little sedimentary structures are observed in the Kuiseb, but some authors (Porada & Wittig, 1983; Kukla et al. 1988) have suggested it resembles a Bouma-sequence with its origins being that of a turbidite succession. The Formation is developed across the entire Damara belt, indicating the connection of the northern Outjo with the southern Khomas Sea (Miller, 2008).

2.6 Intrusive Rocks

2.6.1 Pegmatites and Aplites

Multiple aplite and pegmatite (see section 2.7 for dates) dykes and sills can be distinguished in the region surrounding the Navachab Gold Mine. Sub-vertical NW trending pegmatite and aplite dykes are also commonly observed in the main pit, especially within the silici-clastic units of the Spes Bona Formation. These pegmatite/aplite dykes are very rare in the other pit lithologies such as the Oberwasser and Okawayo Formations.

2.6.2 Mafic Rocks

Numerous dyke- and sill-like mafic rocks have intruded the Damara Supergroup. A prominent metalamprophyric sill set with dyke like offshoots can be observed in the main pit. This metamafic intruded into the Okawayo Fm and overlies the Oberwasser Formations as it intrudes along the contact between the two Formations and expands as dyke swarms from here (Kitt; 2008).

2.6.3 Syn- to post-tectonic granitoids

To the S and SE of the Navachab open pit are numerous syn- to post-tectonic granitoid intrusions. Figure 5 shows the Rotekuppe monzogranite towards the SE and the diorites and granodiorites of the Mon Repos intrusion to the S (Jacob et al. 2000). The Mon Repos diorites and granodiorites are located 5km from the mine as large, medium- to dark-grey plutons. The plutons are zoned as the central parts are dominated by magmatic fabrics and the marginal parts overprinted by contact-parallel solid state fabrics. These intrusions consist predominantly of microcline, hornblende, plagioclase and quartz along with minor amounts of apatite, titanite, zircon and biotite (Jacob et al., 2000). The topographically very prominent Rotekuppe monzogranite is made up of medium grained plagioclase, quartz, microcline, biotite, muscovite and Fe-oxide (Jacob et al., 2000). Recent SHRIMP U-Pb dating of single zircons has put the Rote Kuppe, 539 ± 6 Ma, as being slightly younger than the Mon Repos intrusion dated at 546 ± 6 Ma (Stevens et al. 2014).

2.7 Geochronology

Following findings by Stevens et al., (2014), this section aims to describe the geochronology relationship developed between the mineralisation, igneous and tectonothermal events of the Navachab orogenic gold deposit (Table 3).

There are several diorite and leucogranite intrusions (and related crosscutting aplite and pegmatite sills and dykes) within 5 km of the Navachab gold deposit, but with no direct contact between the mineralised system and any major intrusive body.

Ma	sCZ Tectonothermal events	Navachab
490	Damaran anatexis, migmatites, pegmatites	Rb-Sr biotite in skarn vein
500		494 ± 8 U-Pb titanite in quartz vein
		496 ± 12 U-Pb titanite in lamprophyre
		500 ± 10 U-Pb titanite in quartz vein
510		
520	D2 Deformation Fold Lockup **Au Event at 525 - 520 Ma**	519 ± 2.1 Re-Os molybdenite in quartz vein
		520 ± 2.1 Re-Os molybdenite in quartz vein
530		523 ± 2.1 Re-Os molybdenite in aplite
		525 ± 2.4 Re-Os molybdenite in aplite
540	D2 Deformation Fold Amplification	539 ± 6 U-Pb zircon Rotekuppe granite
550		546 ± 6 U-Pb zircon Mon Repos diorite
560	D1 Deformation	

Table 3: Describes the geochronological relationship developed between mineralisation, igneous and tectonothermal events observed within the South Central Zone, modified from Stevens et al., (2014).

The two closest intrusions, less than 5km from the mine, the Mon Repos diorite and the Rotekuppe granite (Figure 5), have U-Pb zircon ages of 546 + 6 Ma and 539 + 6 Ma. This batholithic-scale granitoid intrusion emplacement coincided with the D2 domal deformational event. Recent Re-Os dating of rare traces of molybdenite from a quartz-tourmaline-rich phalerite+pyrite–bearing aplite and a more 'normal', but molybdenite-bearing, aplite yielded Cambrian Re-Os ages of 525.2 + 2.4 Ma and 523.0 + 2.1 Ma, respectively. Molybdenite-bearing, NNE-dipping, extensional auriferous quartz+bismuth+pyrite+pyrrhotite veins (dominant set), with garnet selvage, have Re-Os ages of 520.0 + 2.1 Ma and 519.4 + 2.1 Ma (Table 3). It's easily noted that the dates for the aplites and quartz veins (Navachab mineralisation) are within error, cross-cutting relationships however indicate that aplite intrusions are generally younger than the

quartz veins. Low-angle to highly cross-cutting sheets of meta-lamprophyre occurs in the central parts of the Navachab open pit. An U-Pb titanite age of 496 + 12 Ma from the metalamprophyre is suggested to represent a thermal event causing the re-setting of titanite ages. The U-Pb titanites ages of 500 + 10 and 494 + 8 Ma of mineralised quartz veins at Navachab are interpreted to correspond to a metamorphic recrystallisation event associated with a thermal pulse at the end of the Damaran High-Temperature-Low-Pressure (HTLP) event. A biotite from the margin of a skarn vein at Navachab yielded an age of 490 Ma, interpreted to be a cooling date.

Widespread anatexis, partial melt development and pegmatite emplacement in the lattermost stages of the Damaran orogeny suggest that, after auriferous vein development at 525 – 520 Ma at Navachab, subsequent gold redistribution and even ore mineral melting (notably the relatively low temperature gold-bismuth minerals) occurred, Stevens et al., (2014). The timing of the Navachab gold mineralisation at 525-520 Ma coincides with peak T conditions and widespread anatexis in the lower crust of the southern Central Zone and granite and pegmatite emplacement at mid-crustal levels. This temporal and spatial relationship suggests that late-tectonic peak metamorphic conditions and associated plutonism played a critical role in the development of the Navachab hydrothermal system.

Chapter 3: Mine Geology

3.1 Introduction

This study focuses on the Footwall (Spes Bona Formation) of the Navachab open cast pit. The sedimentary sequence, known locally as the Footwall (FW) sequence or Lower Schist (LS), consists predominantly of intercalated quartz-biotite schists and calc-silicate felses. These subunits are economically mineralized by quartz-sulphide veins (mm to cm thick) of different structural orientations.

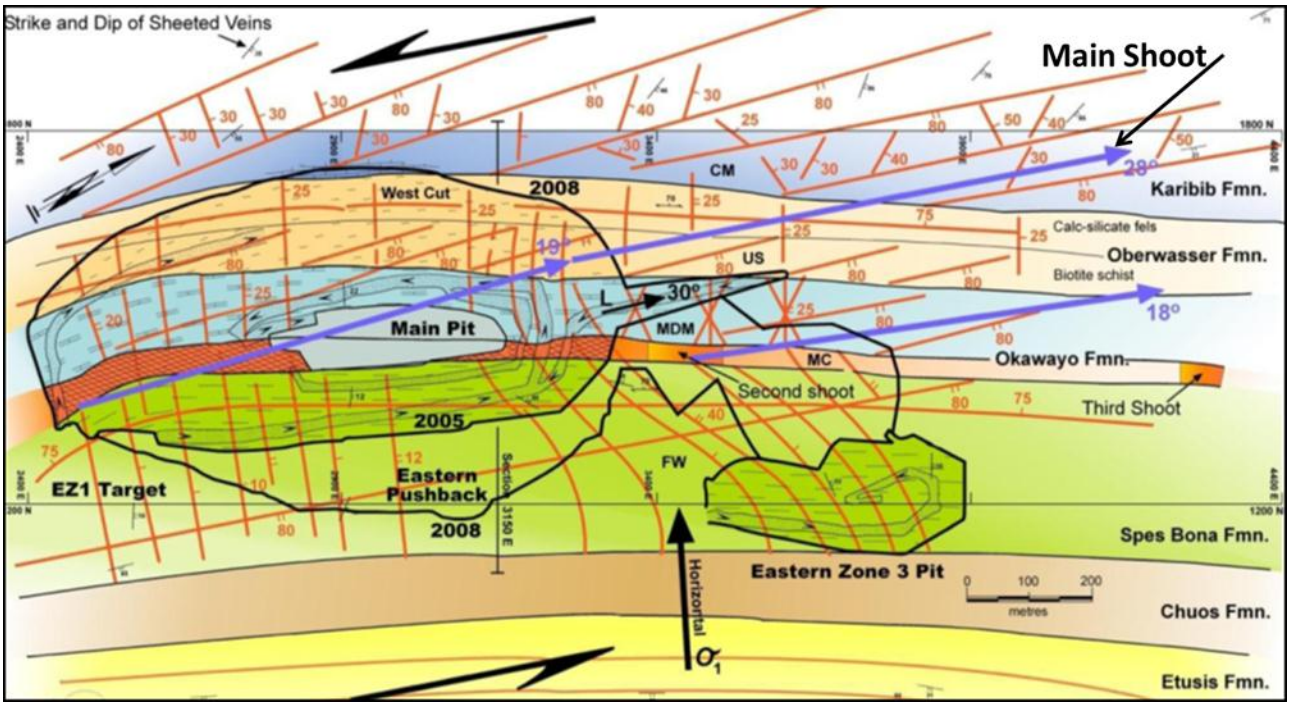

Figure 10: A simplified geological map of the Navachab open pit showing the main pit and contained lithological formations. The blue arrows show the plunge of the Main, Second and possible Third en-echelon ore shoots. The Spes Bona Formation, in the east, contains mineralized quartz-sulphide veins that form part of the Main Shoot ore body (Internal report by Rockwater Consulting, 2008).

The FW mineralization forms part of the main Navachab ore body, the Main Shoot is elongated and plunges at shallow angles (ca. 20-30°) towards the NNE (Figure 10). The plunge of the ore shoots coincides with the plunge of the local fold axis of the regional hosting structure to the deposit, the Karibib Dome. The Karibib Dome is a doubly

plunging, NNE-SSW trending and NW verging anticline almost 5 km in diameter, the Navachab gold deposit is situated within its steeply dipping NW-limb (Figure 5).

3.2 Lithology of the Navachab Open Cast Pit

The Navachab open pit cuts perpendicularly through the central formations of the Damara Supergroup (Table 2). This orientation provides the observer with a cross sectional view of the Oberwasser Formation in the west, to the Okawayo and Spes Bona Formations in the east (Figure 11). This study focuses on the latter, The Spes Bona Fm, while providing necessary insights to the Okawayo and Oberwasser Formations.

Figure 11: A schematic diagram of the Navachab open pit looking to the NNE. The lithological formations exposed include the Spes Bona, Okawayo and Oberwasser which all dip steeply towards the WNW (to the left of the diagram). Mineralization is hosted by quartz-sulphide veins crosscutting the sub-vertical lithologies. The host rocks are intruded by numerous pegmatite, aplite and lamprophyre dykes with concordant and discordant contact relationships (from Kitt, 2008).

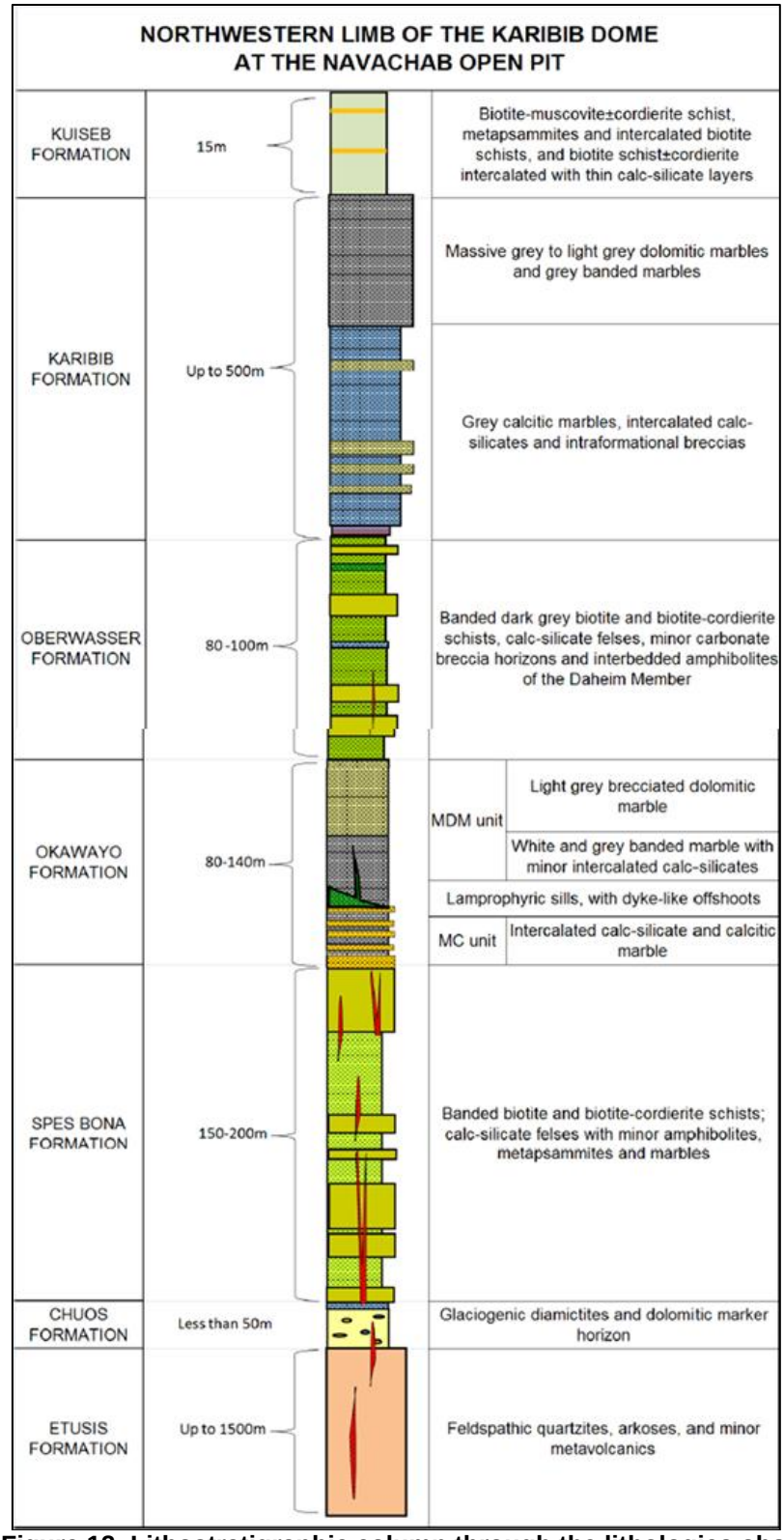

Figure 12: Lithostratigraphic column through the lithologies observed within and around the Navachab open pit (after Kitt, 2008). The red intrusions schematically represent aplite and pegmatite intrusions.

3.2.1 The Spes Bona Formation

The formation represents the lowermost sequence of the Swakop Group exposed in the Navachab open pit. Intercalated layers (from mm to m scale thicknesses) of biotite schists +- cordierite and calc-silicate felses dominates the formation that can reach a thickness of up to 200m (Figure 12). Individual schist layers range between 0.5cm and 15m in thickness, while calc-silicate layers reach maximum thicknesses of only 1m. The formation has a light grey weathered colour (Figure 13), but is darker grey on freshly struck surfaces.

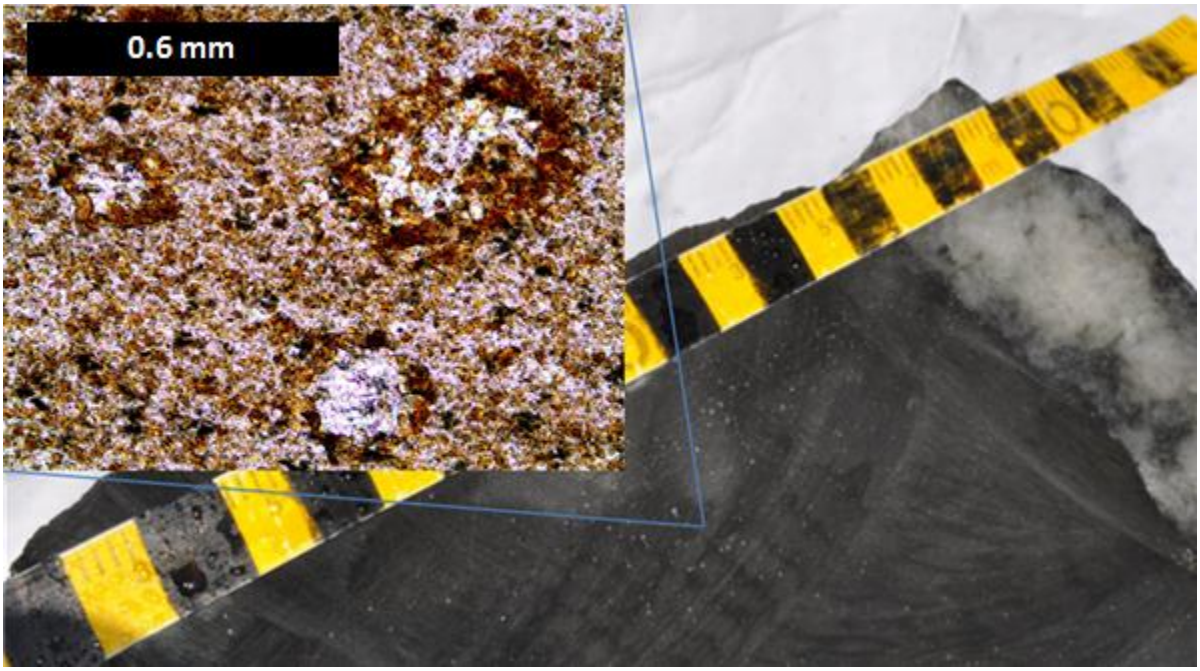

Figure 13: Shows a fresh rock specimen and thin sectional of the biotite schist. Note the oval biotite rings with quartz cores, the section is 1.25mm wide.

The biotite schist layers are fine grained, consisting of biotite (50%), quartz (10%), K-feldspar (20%), cordierite (10%) and plagioclase (10%). These minerals are sub- to euhedral in shape with an occasional spotted texture brought about by oval-shaped aggregates (about 0.3 cm diameter) of biotite and quartz (Figure 13). The aggregates

are interpreted as decomposition textures after cordierite. The preferred orientation of boitite within the schists displays a well-defined foliation within the layers.

The Calc-silicate rocks are light to dark green, medium- to fine-grained felses consisting of clinopyroxene/diopside (35%), plagioclase and K-feldspar (30%), biotite (10%), quartz (10%), actinolite (10%) and sphene (5%), Figure 14. Actinolite was observed to replace clinopyroxene but it is unclear if all actinolite is of secondary origin or if primary (peak metamorphic) actinolite is present as well. These felses are massive and weather positively to the surrounding rocks.

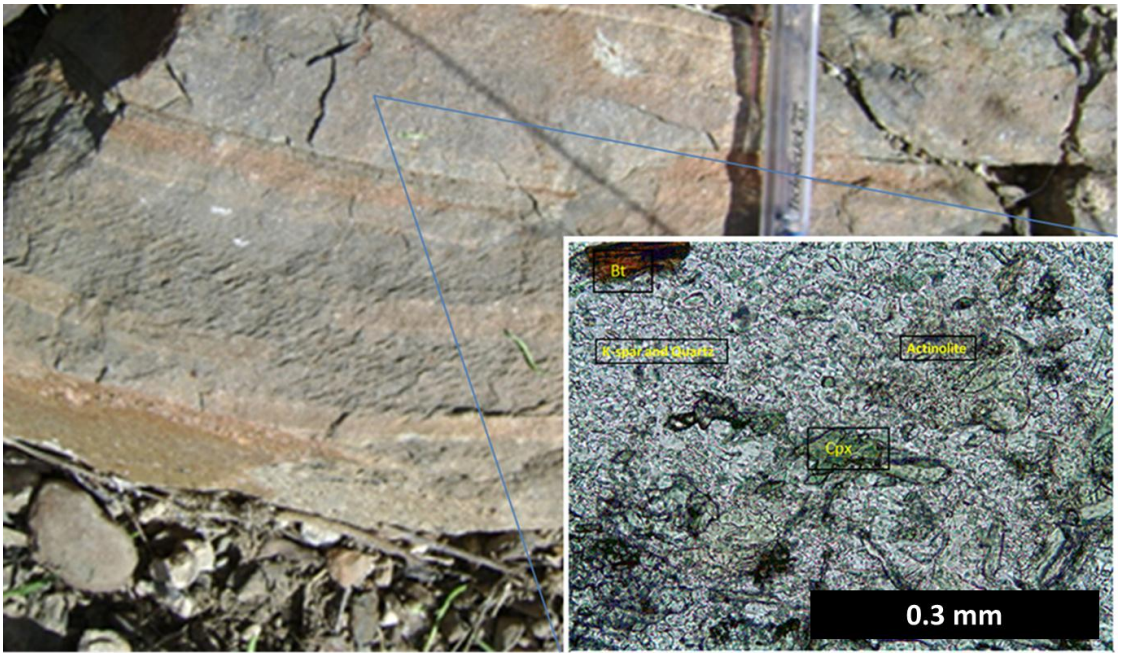

Figure 14: Shows a fresh rock specimen and thin section of the calc-silicate sub unit. The thin section is 0.6mm wide.

In the Spes Bona Formation biotite schists are generally more abundant than calc-silicate rocks. The compositional layering coincides with the foliation in the Navachab area. The transition between biotite schists to calc-silicate rocks can be abrupt, gradual or calc-silicate rocks and biotite schists can be pervasively intermingled.

3.2.2 The Okawayo Formation

The overlying Okawayo Formation is a 150m thick marble sequence that can be devided into two parts. The upper part is about 110m thick and consists of calcitic marbles and minor intercalations of dolomitic marble. The basal part of the formation overlying the Spes Bona Formation is known as the MC unit. The 40m thick sequence of intercalated calc-silicate felses and calcitic marbles plays host to the high grade massive sulphide ore bodies of the Navachab Gold Mine. The contact between the upper and basal parts is marked by the intrusion of a mafic lamprophyre sill (Figure 12).

3.2.3 The Oberwasser Formation

Also known as the Upper Schist or hangingwall of the Navachab open pit, this formation is 100m thick and very similar to the Spes Bona Formation. It consists of primarily of interbedded biotite schists and calc-silicates felses with minor marble bands and amphibolites.

The biotite schists are made up of fine grained biotite, cordierite, plagioclase, K-feldspar and quartz while the calc-silicates consists of diopside, plagioclase, K-feldspar and minor biotite and quartz minerals.

3.2.4 Intrusive rocks

The Navachab open pit and especially the Spes Bona Formation are intruded by numerous generations of aplites and pegmatites (Figure 11 & Figure 12). These subvertical NW trending intrusions range in widths between 1cm and 5m. Most pegmatites relate to late-D2 tectonics as they cross-cut the mineralized quartz veins. However, on rare occasions these intrusions are observed to have undergone boudinage, folding and are cross-cut by some quartz veins. This suggests that, at least, the later stages of mineralization were related to plutonic activity in the region.

Figure 15, A aplite dyke in the FW sequence cross-cut by a shallowly dipping quartz vein (top) as it cross-cuts another shallowly dipping vein (bottom). This suggests the intrusion of felsic dykes swarms and quartz veins were syn-genetic.

3.3 Structural Geology of the Navachab Open Cast Pit

The main structural elements of the study area are listed in Table 4. Planar penetrative fabrics (S), linear penetrative fabrics (L), folding of planar and linear fabrics (F) and deformation phase (D) are attached to suffixes (0, 1, 2 etc.) describing the structural order determined by evaluating overprinting and cross cutting relationships between different fabrics.

The Navachab Gold mine is situated on the NW limb of the Karibib Dome structure. It has a prominent NW fold vergence as a result of a steep-dipping NW limb and shallow-dipping SE limb. The doubly plunging, 12km by 4km wide anticline belongs to a progression of similar NE trending dome structures found across the sCZ. The sub-

vertical rocks of the open pit dip steeply towards the WNW, with an average dip and dip direction of 75°/291° (Figure 16).

Deformation Phase	Fabric Element	Field observations
Primary	S0	Primary bedding as a result of sedimentary deposition
D1, low angle shearing.	S1	Bedding sub-parallel foliation in schistose units, bedding transpositioning
	F1	Intrafolial folds best observed within the marble units of the Okawayo Formation
D2, top to NW trusting causing NW-verging folds.	S2	Sub-vertical to steep SE dipping, NE-SW trending, axial planar foliation of F2 folds.
	F2a	1st order doubly plunging Karibib and Usakos fold structures (domes).
	F2b	2nd to 4th order fold structures, varying from hundreds of meters to cm scale.
	L2f	Shallow NE plunge of fold hinges of lower order F2 folds.
	L2m	Shallow NE and SW plunge of mineral and marble breccia stretching lineations.

Table 4: Fabric elements that can be ascribed to the main deformation phases, D1 and D2 are summarized (after Kitt 2008).

D1 is observed within the schistose units of the Spes Bona and Oberwasser Formations as a bedding sub-parallel foliation (S1). The marble units of the Okawayo Formation are primarily recrystallized, but in zones where bedding/banding is still preserved its interpreted to be refolded tight- to-isoclinal intrafolial folds (F1). These F1 folds thus preserve the S1 fabric as a transposition fabric (S0/S1) developed in marbles.

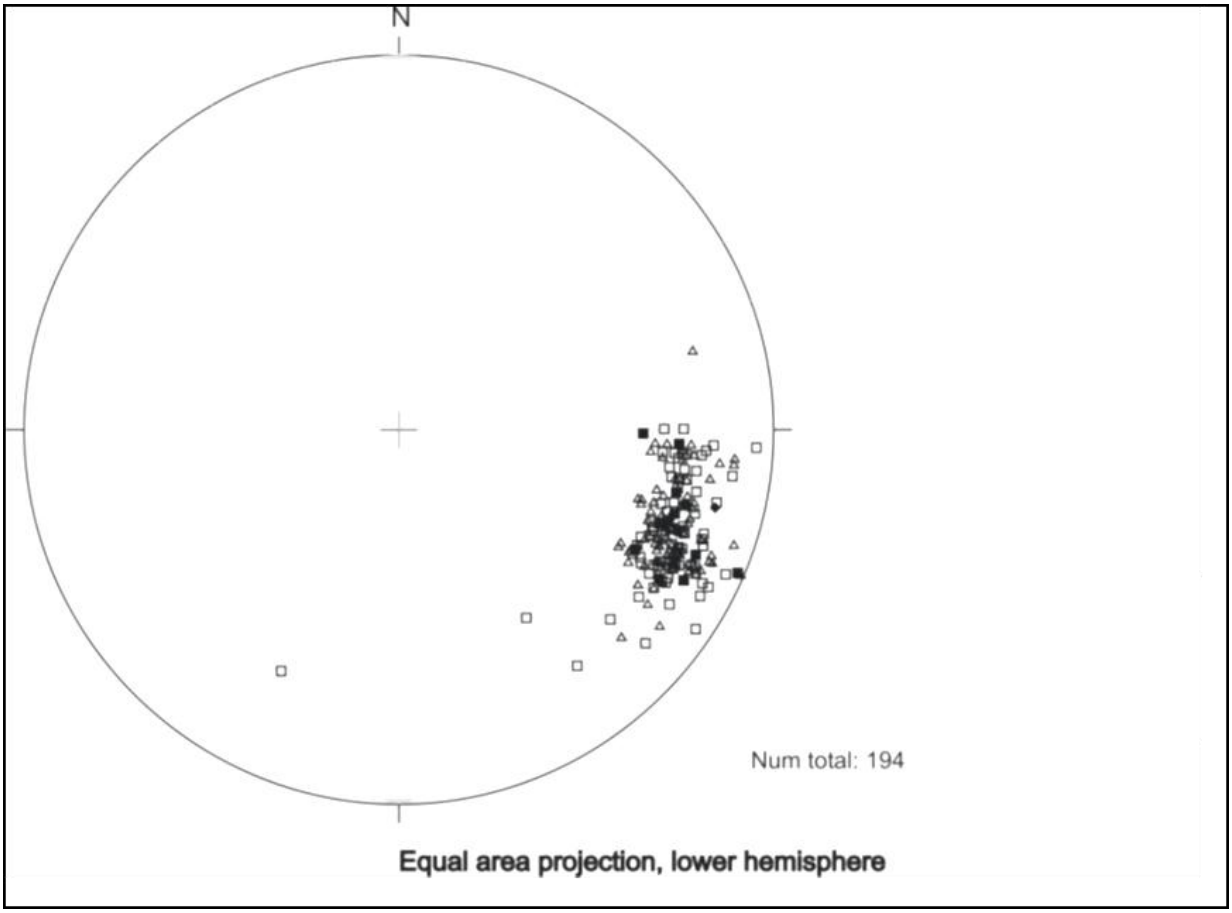

Figure 16: A stereographic projection of poles to the plane bedding readings taken along the FW sequence. The S0 foliation (bedding) observed in the Navachab open pit is relatively uniform as no secondary folding (F2b) is present.

The later D2 event is associated with dome formation (F2a), e.g the Karibib dome, resulting in the refolding of earlier D1 fabrics. Lower order F2b folds are observed within the schistose and marble units to the NW of the open pit. These folds are asymmetric with varying wavelengths and amplitudes (ranging from a few mm to several meters), they trend parallel to the first-order dome structure (F2a) while plunging towards the NE. A sub-vertical axial planar foliation (S2) is observed within the F2b folds which, on occasion, plays host to quartz vein formation. Sub-vertical dolomitic marble and calc-silicate units are often deformed into symmetrical, chocolate-tablet type boudinage structures due to the occurrence of sub-horizontal shortening normal to S2 and bedding.

Displacement in the open pit is observed where faults off-set host units and occasionally, their contained mineralization. These fault structures usually develop sub-parallel to the layering/bedding, although shallow dipping faults do occur (Figure 17). The faults are characterised by calcite veins and brecciation of the host rock into angular pieces with a white, sometimes sparry calcite matrix. In places, chlorite is also associated with these faults. The faults are considered to be later than the gold mineralisation since they show a more brittle type of deformation, greenschist facies minerals (calcite, chlorite) and crosscut the veins (or sometimes run along the contact between a vein and its alteration zone). In drill core the displacement observed is minor (in the range of few cm), but larger fault structures do occur in the study area. This late stage faulting is linked to the redistribution of earlier ore bodies, especially in the FW sequence. The absolute effect and scale of displacement is not yet fully understood.

Figure 17: A) displacement of a quartz vein in biotite schist by brittle faulting, note the calcite veins within the fault plane. B) Two quartz veins in calc-silicate felses being displaced by ductile shearing. C) More brittle deformation observed in a quartz vein hosted by biotite schist, note the absence of calcite veining. D) 7cm thick fault breccias consisting of broken up schists and calc-silicates, quartz vein material and late stage calcite fillings. E) Quartz vein in biotite schist with intercalated layers of calc-silicate rock (greenish bands). This is a rare example where displacement of the host rock is observed along a vein. Scale bar is in mm.

3.4 Quartz veins in the Footwall

Quartz-sulphide veins in and around the Navachab Gold mine have been studied to great depths in recent years with all key (to the Au mineralization) vein sets well documented, see Kisters, (2005), Wulff (2008) and Kitt (2008).

Most authors agree that the so called conjugate vein set plays the primary role in hosting the gold mineralization while all other vein sets are only of subordinate importance. This study aims to understand to what extent the secondary vein sets add value to the resource.

From the FW sequence, ten diamond drill holes were selected for detailed structural work. Hole selection criteria aims to provide a good representation of the FW as it is contained within the main open pit (Figure 18A and B).

The 10 holes were drilled sub-horizontally, azimuth 135˚, inclination -5˚, to intersect the FW perpendicularly. This presents the observer with a cross sectional view of the sequence, providing an optimal orientation for measuring vein orientations, bedding and other structural elements (Figure 18C).

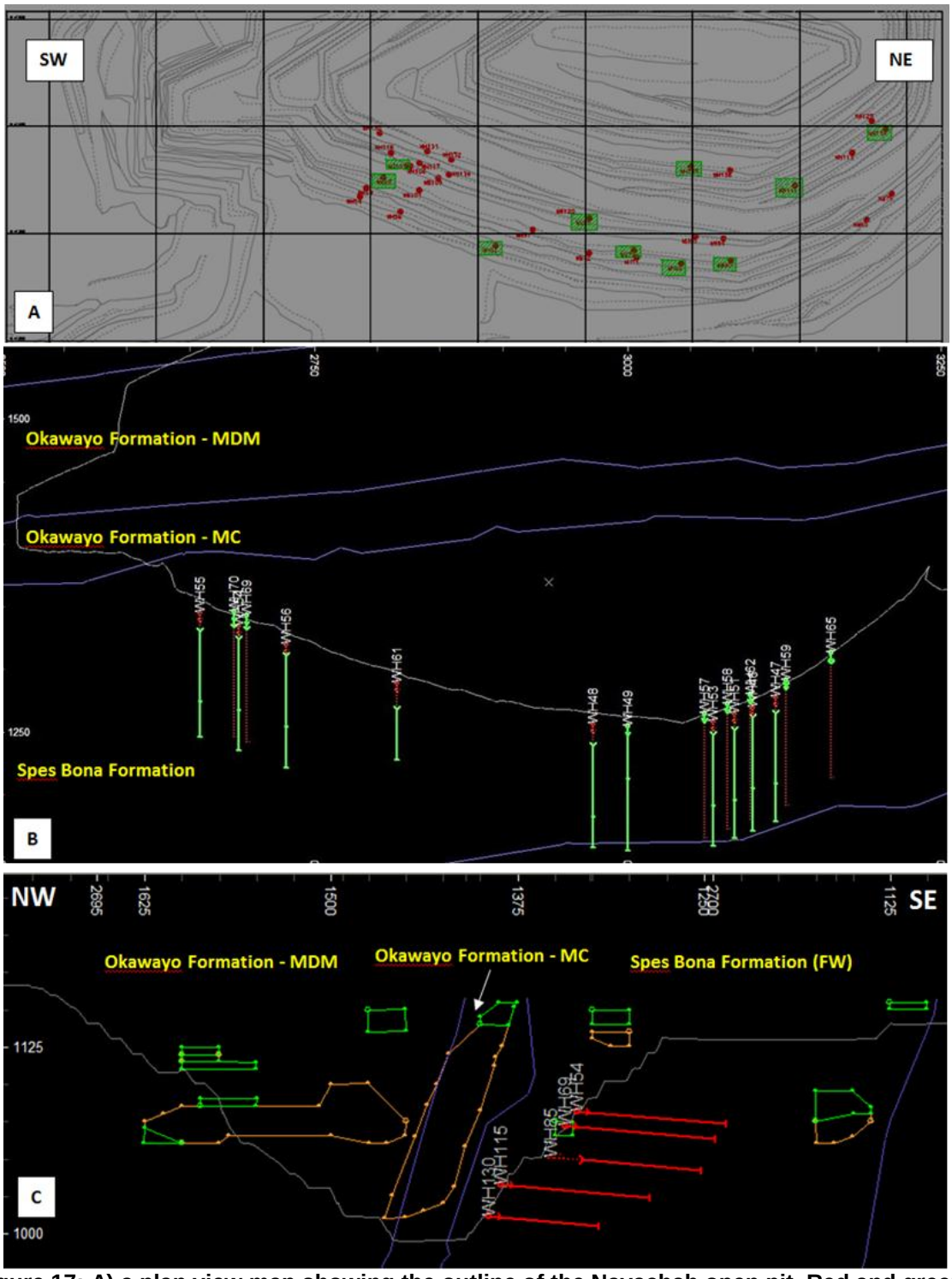

Figure 17: A) a plan view map showing the outline of the Navachab open pit. Red and green marks represent all selected diamond drillholes used to gather petrographical (red and green marks) and structural (green marks) data in the study. B) Is a plan view level map, modelled in Datamine, of level 1075. All holes were drilled perpendicularly into the FW sequence. C) Is a cross section of the main pit along section line 2700, looking towards the NE. The pit outline in grey with lithological contacts drawn in blue, orange and green wireframes represent ore envelopes and in red are some of the holes used for this study.

3.4.1 Quartz Vein Geometry

From the 10 selected drillholes, 1456 quartz-sulphide veins were structurally measured and the data displayed on stereographic projections. These are plotted on the lower hemisphere of an equal-area stereonet (Schmidt projection). The stereographic plots were interpreted in order to identify the different quartz vein sets contained in the study area (Figure 19 & 20). The three main quartz vein sets (Figure 19) identified in the FW sequence are:

1. a conjugate vein set (CVS) consisting of 2 main vein arrays with shallow dips (between 5˚ and 40˚) towards the NE and NW respectively,
2. a set of steeply (56-89°) WNW-dipping, bedding/foliation parallel veins (BPV) with an average dip direction of 293˚/75˚ and
3. a S2 fold (Karibib dome) axial planar vein set (S2V) dipping steeply (75-89°) towards the SE.

Figure 18: Stereographic contour plot of poles to the plane from planar vein orientations readings taken on the 10 selected holes. Note the strong bias towards the bedding parallel and S2 (axial planar) vein sets due to the horizontal drilling orientation. The black half circle defines the average dip (73˚) and dip direction (293˚) of bedding S0.

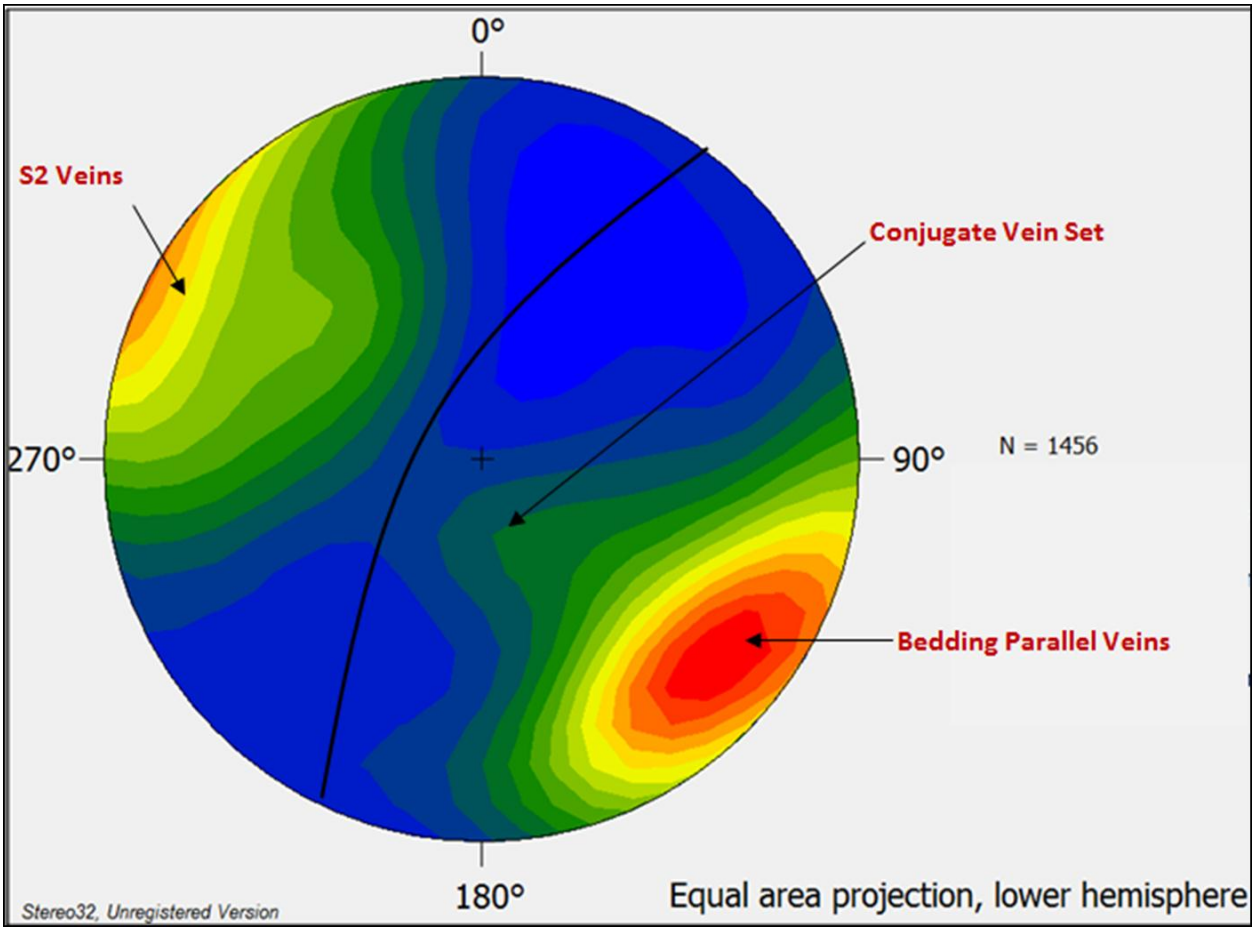

The horizontal drill orientation of the selected holes developed a strong bias primarily exposing quartz veins that are orientated at steep angles (vertical structures) to the drill direction (Figure 20). The bedding parallel vein set (BPV) and S2 veins (S2V) were intersected at regular intervals while the conjugate veins (CVS) trending parallel to the drill string not.

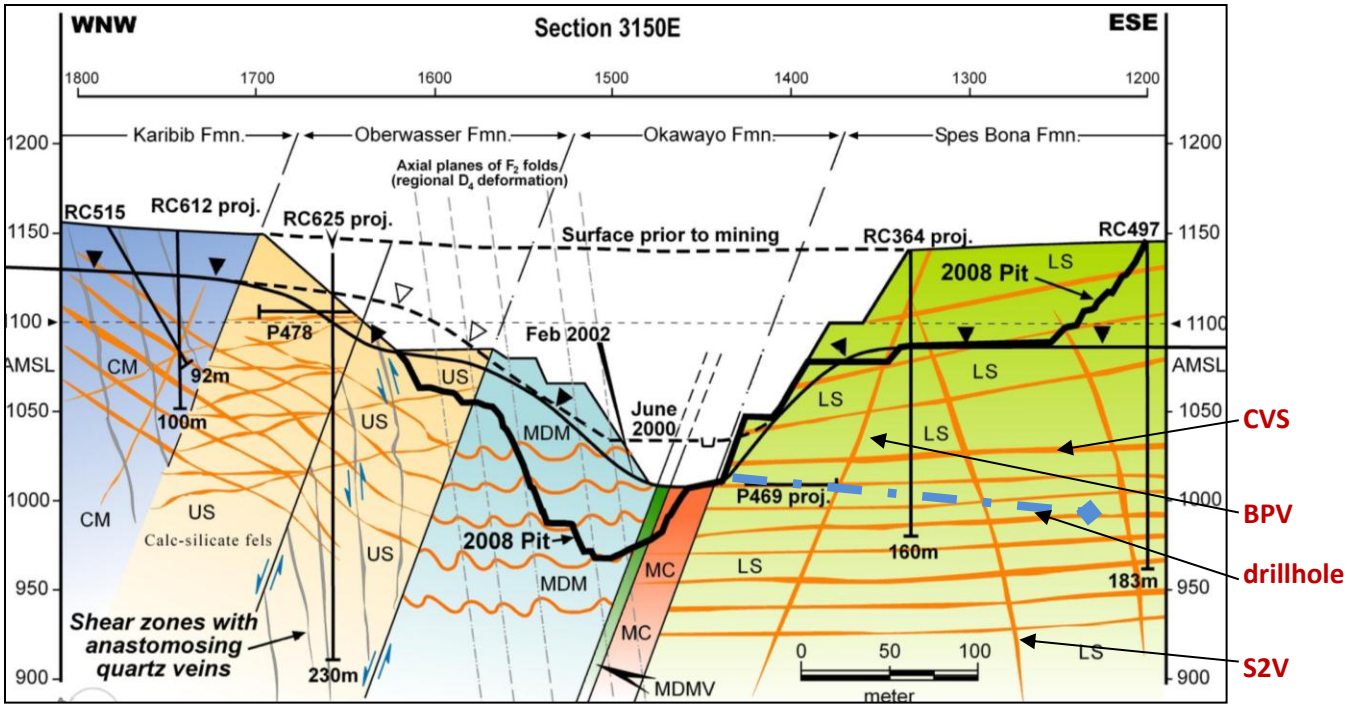

Figure 19: Shows a cross section, looking NNE, thru the Navachab Main Pit with the different lithologies demarcated. The three main quartz vein sets, as they occur within the Spes Bona Formation, are schematically represented along with a drill line showing the general azimuth and dip of the holes drilled for this study. From a Navachab internal report, 2008.

The bias effect resulted from the drill orientation and subsequent angle whereby veins were intersected, evident in Figure 19.In order to correct for the bias observed, historic vein orientation measurements (623 in total) gathered from FW mapping exercises and work done on vertically drilled, into the FW sequence, core was combined with the original study data. The historic data again shows a bias trend towards the CVS (Figure 21A) as pit mapping and vertical drill core primarily exposes horizontal features (the conjugate vein set).

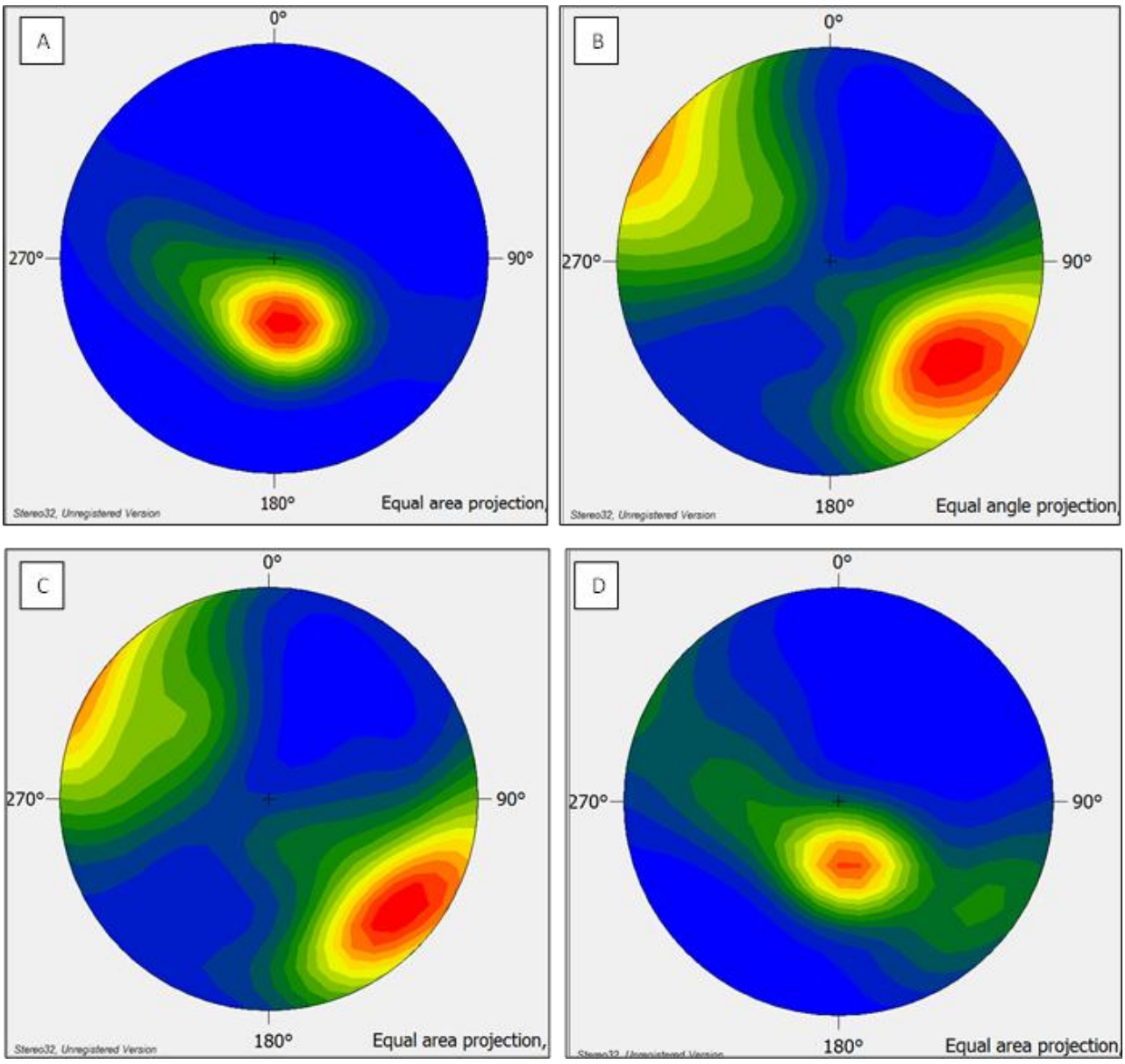

Figure 20: A) A contour plot of poles to the plane of historic vein orientation data gathered from pit mapping and vertically drilled core from the FW sequence. Note the strong bias towards the horizontally trending CVS.

B) Demonstrates a pole to the plane contour plot of the statistically halved data set, including 728 quartz vein measurements.

C) Is the original data set with 1456 vein measurements plotted. Although B only represents half the data it still accurately represents the original data set.

D) The combined data set of 1351 vein measurements represents the three main quartz vein sets as they occur within the FW sequence.

To accurately merge the two proportionally different data sets, the original study data, consisting of 1456 vein measurements, was statistically halved to 728 readings. Figure 21B and C shows this process maintained the integrity of the original data set.

The combined data set consist of 1351 quartz vein measurements, providing an accurate representation of the different quartz vein sets hosted by the Spes Bona Formation (Figure 21D). Making up the largest portion of auriferous quartz veins in the FW, the conjugate quartz vein set (CVS) constitutes 38% (531 veins) of the total number of veins measured (Figure 22). The bedding parallel (BPV) veins follow with 22% (300 veins) and the S2V with 17% (229 veins). All other veins with unrecognised orientations contribute to 22% (291 veins) of veins measured in the FW.

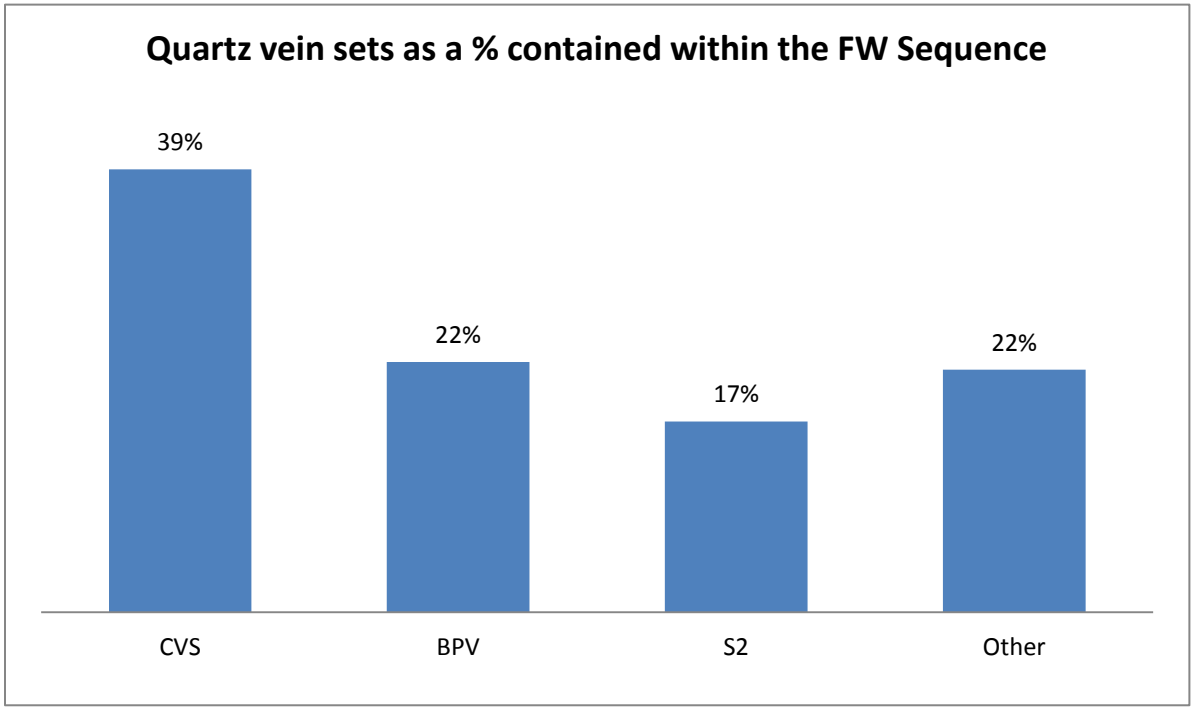

Figure 21: A bar graph with vein set % as hosted within the FW sequence.

3.4.2 Quartz vein morphology

The following section describes morphological features observed for veins of all 3 main vein sets.

Mineralogy

The quartz-sulphide veins consist primarily of quartz, pyrrhotite and chalcopyrite minerals easily identifiable with the naked eye. Microscopically, minor amounts of clinopyroxene (often replaced by secondary actinolite and calcite), K-feldspar and carbonates, as well as sphalerite, arsenopyrite, native bismuth, native gold bismuthinite and Bi-tellurides were observed (Figure 23) Wulff, 2008. Gold commonly occurs as small grains (few µm to 0.1 mm) of free gold closely associated with other ore minerals, especially Bi-tellurides, and surrounded by quartz. Larger grains ("nuggets") of gold are very rare but have occasionally been found.

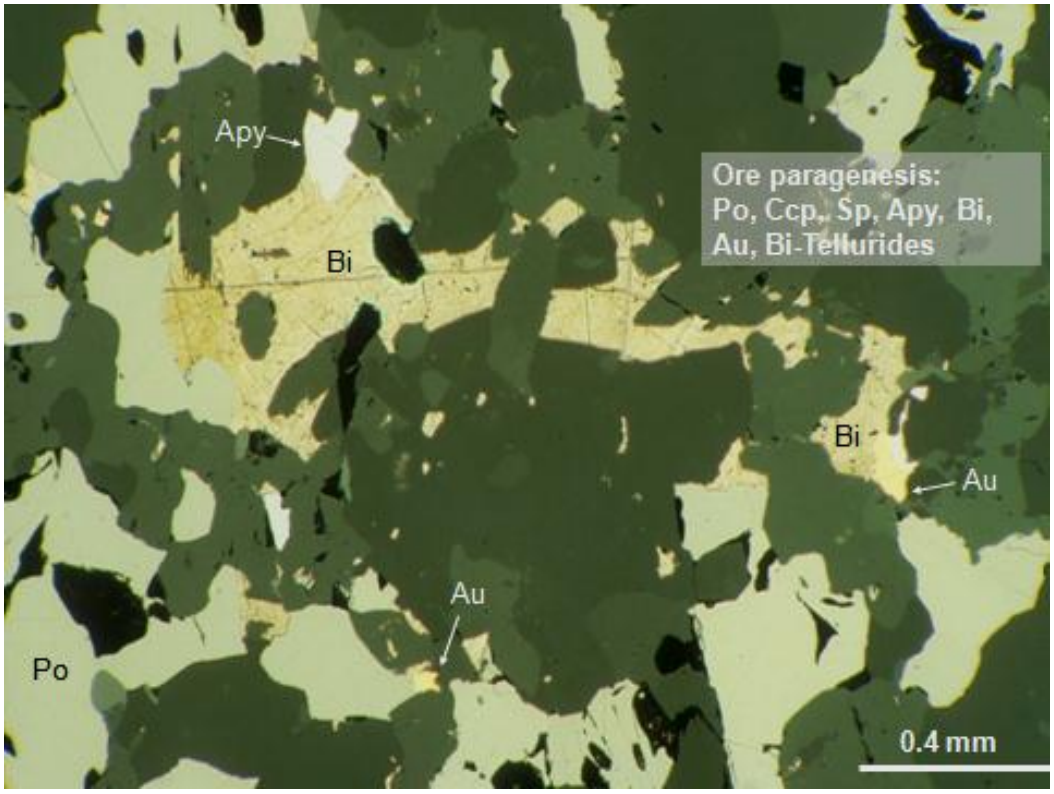

Figure 22: Ore paragenesis quartz-sulphide veins, observed under a reflective light microscope (after Wulff, 2008).

Thickness and Distribution

Veins measured in this study range in thickness from less than 1cm to up to 1m, but on average are between 2 and 5cm thick. Veins can be followed for over 300m down dip as they appear straight with very little thickness variations, showing remarkably high length-to-thickness aspect ratios of >> 1000:1 (Kitt, 2008). Vein terminations are associated with the thinning of one vein as an adjacent vein thickens, demonstrating a degree of hydraulic connectivity within the vein system.

Veins are in sharp contact with their siliceous hosts and include no wall rock slivers. The spacing between veins varies from a few cm to several m. Depending on the location within the FW, veins are more concentrated as they usually occur in clusters with distributions of several veins (~ 3-7) occurring over a 10m core spacing. Clustered areas are bounded by less populated zones usually not exceeding a width greater than 10m. The interplay of veined and less veined zones is a likely result of strain shadows occurring within the host rocks. Fracturing and vein formation is favoured in zones with existing veins, before initiating in intact wall rock (Kitt, 2008).

Alteration

Quartz veins are surrounded by mm to cm thick alteration zones/selvedges. Alteration may also extend up to several meters into the host rocks following fractures and bedding plane boundaries. The degree of alteration does not relate to vein thickness. Observed alteration mineralogy varies down strike, between neighbouring veins or might be the same for all veins within a cluster.

Following Wulff 2008, two major alteration types are developed around veins located in biotite schist and one type in the calc-silicate units of the FW sequence. Garnet-biotite alteration and Actinolite-quartz alteration, figure 24, develops primarily around veins

hosted in schistose units. Garnet-biotite-alteration developes as the host rock is replaced by garnet, with associated biotite and minor K-feldspar. Actinolite alteration is charecteristerised by large porphyroblasts of actinolite (up to 20% of the alteration zone) and minor feldspar, calcite, biotite and titanite (Kitt, 2008).

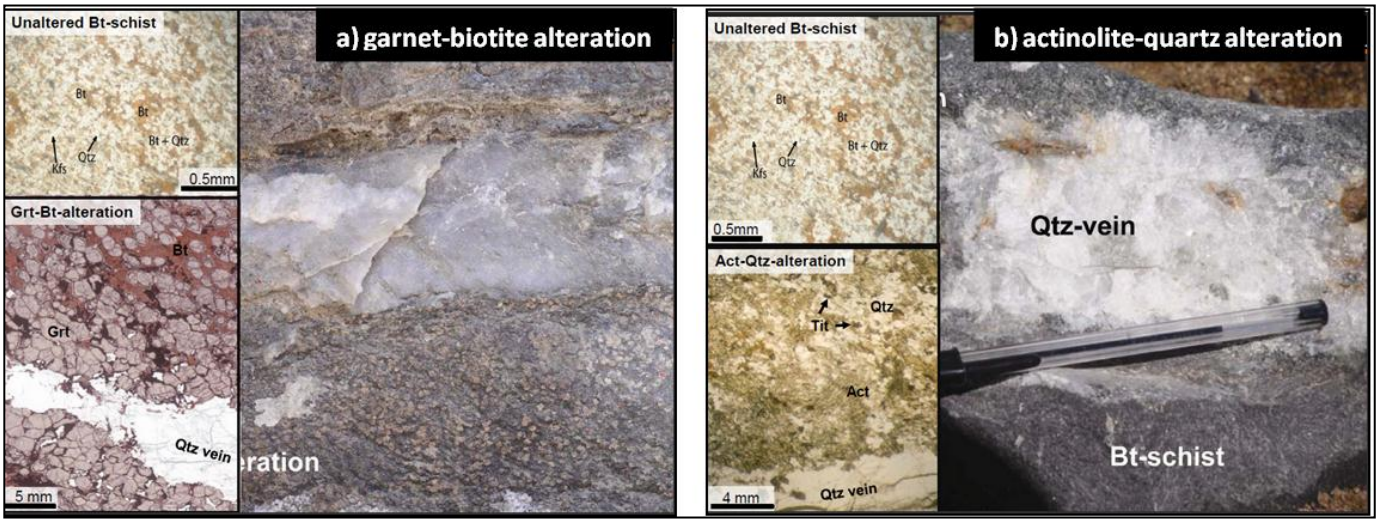

Figure 23: A) Represents the garnet-biotite alteration type observed in a hand specimen (right). On the left, and a comparative view from under the microscope is provided between altered and unaltered biotite schist of the FW sequence. The same was done for (b) where actinolite-quartz alteration is represented under the microscope and in a hand specimen (from a Navachab internal presentation).

In calc-silicate layers garnet-clinopyroxene (±K-feldspar ±quartz) alteration is locally present. Different variations of the above mentioned alteration occurs as some veins are without any alteration paragenesis, or when biotite alteration solely forms instead of fully developed garnet-biotite alteration and, where biotite schist develops pervasive silisifiction or bleaching around quartz veins instead of fully developed actinolite-quartz alteration.

These alteration zones are erratically mineralized, containing the same ore minerals observed in the quartz veins. High grade quartz veins result in better graded alteration zones, but with lower gold concentrations opposed to the adjacent vein, (Wulff 2008).

Vein Textures

The FW quartz veins are massive, predominantly composed of blocky, annealed (ductile and statically) re-crystallized quartz minerals with subordinate fine grained carbonates and K-feldspar. Veins are made up of smoky grey or milky to clear quartz. Microcracks are common as they develop perpendicularly to the vein boundaries. These are highlighted by chalcopyrite and pyrrhotite fills.

Vein Deformation

Veins occurring in the FW sequence have undergone post-emplacement deformation where veins are folded and boudinaged. Folding is primarily observed in veins orientated at steep angles to bedding, the conjugate vein set (Figure 25). The folding present here is referred to by Kisters (2005) as F2b folds. These NE trending folds record a co-axial shortening strain developed at high angles (perpendicularly) to the steep bedding on the NW limb of the Karibib dome, Kitt (2008).

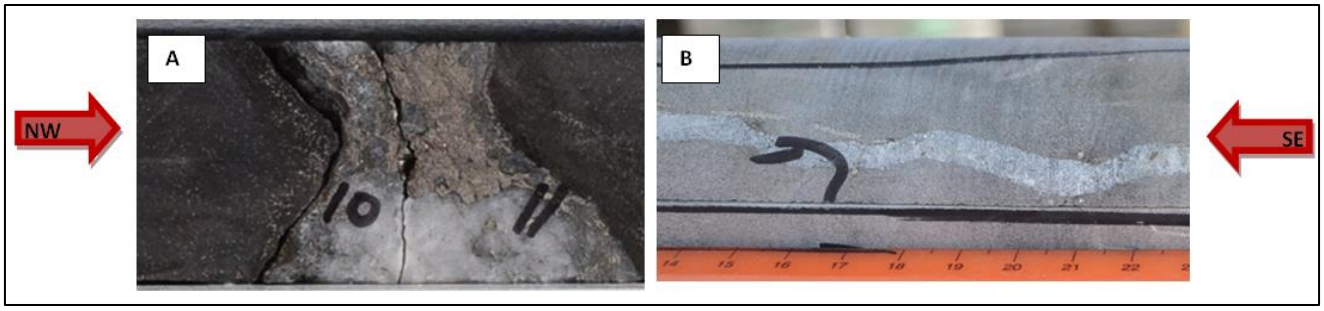

Figure 24: A) Shows a boudinaged bedding parallel vein with remobilised pyrrhotite concentrated in the boudins neck, the neck is 2cm across. B) Illustrates folding in a conjugate vein cross-cutting bedding at steep angles, scale is in cm. Red arrows indicate the co-axial shortening strain developed at high angles to the bedding, the regional shortening strain.

The same regional, sub-horizontal shortening strain resulted in bedding parallel veins being boudinaged as the rock package extended/thickened vertically. The boudins are rectangular shaped or may show 'pinch and swell' structures (Figure 25) which are rarely separated. Coarsely recrystallized pyrrhotite and chalcopyrite are concentrated in boudins necks which indicate post-emplacement sulphide remobilisation.

3.5 Mineralization Evolution

Quartz veins were emplaced during folding and fold amplification of the Karibib Dome, Kisters (2005). This correlates to the late stages of the D2 event, associated with NW-SE directed, sub-horizontal shortening resulting in regional top-to-the-NW thrusting and NW-verging folding.

Local lithological and structural controls, however, still play an important role in developing economic grade mineralization. Timing of the mineralization event occurred between 525 to 520 Ma, see section 2.7 after Steven et al 2014.

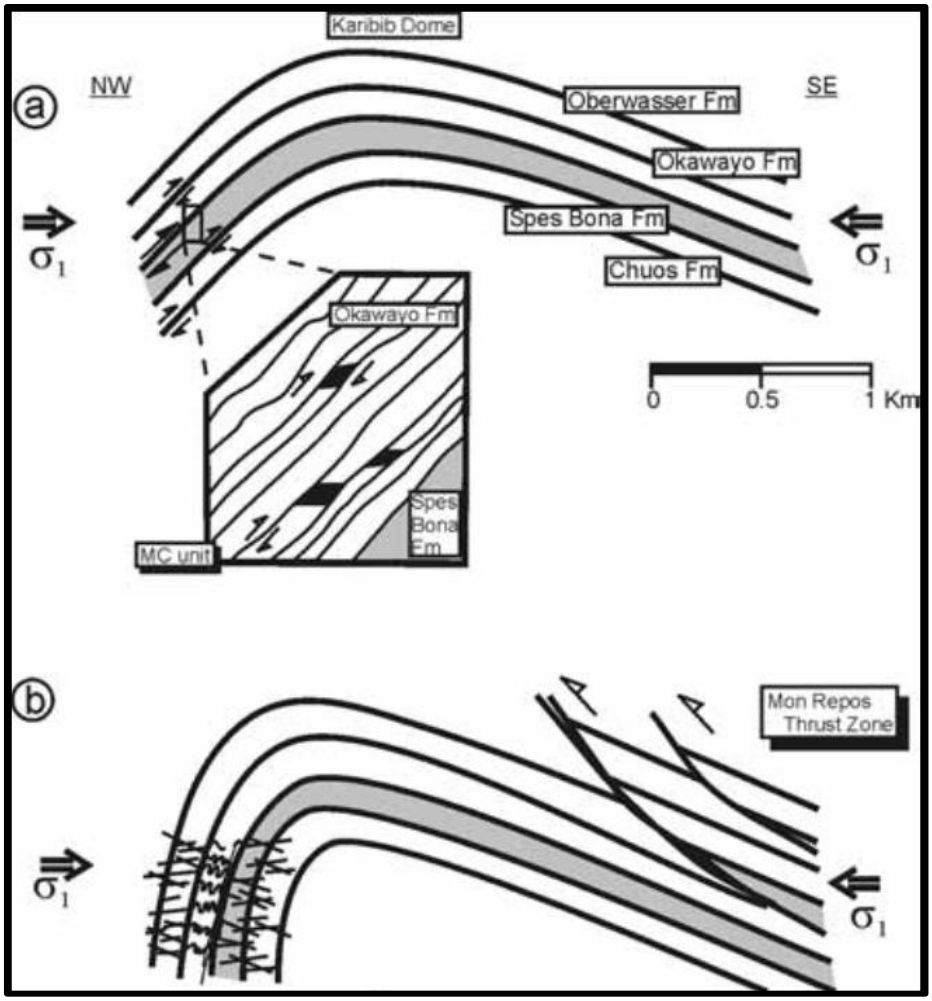

Figure 25: Cross-section cartoon of the Karibib Dome during regional NW-SE directed shortening. A) Represents amplification of the Karibib Dome, where flexural flow along bedding contacts developed a plumbing system for the BPV set. B) Depicts fold lock up and the development of extensional fractures sucking in over-pressurised hydrothermal fluids to form the CVS (from Kister, 2005).

Kisters (2005) proposed a model for fracture development bringing about the Navachab quartz vein swarm (Figure 26). During fold amplification of the Karibib dome, flexural flow along bedding-parallel slip planes resulted in fracture/weak planes developing along bedding contacts. These bedding plane fractures form the fluid plumbing system hosting the bedding parallel vein set. Fold amplification continued to rotate the NW limb to sub-vertical attitudes resulting in fold lock up and the deactivation of bedding parallel flexural slip. Fold lock up and the continuation of NW-SE directed crustal shortening facilitated the development of sub-horizontal extensional fractures. These extensional fractures sucked in gold bearing over-pressurised hydrothermal fluids resulting in the development of the S2 and conjugate vein sets.

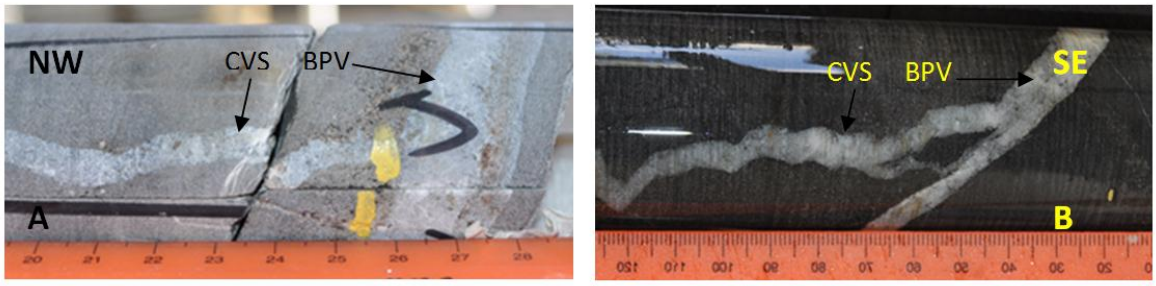

Figure 26: A and B are pictures representing the genetic relation between the CVS and the BPV set. In (A) bedding parallel veins developed after the formation of conjugate veins and in B the different sets developed concurrently. These observations propose bedding parallel veins developing syn- to post-genetically with the conjugate vein set. Note how in A the BPV displaced the CVS and the pronounced folding of the CVS.

Following this model, cross-cutting relationships developed between sub-horizontal (CVS) and sub-vertical (BPV) veins should display an uncomplicated genetic sequence, where conjugate veins cross-cut earlier bedding parallel veins. This study however found cross-cutting relationships portraying two different scenarios where 1) bedding parallel veins cross-cut conjugate veins, and 2) conjugate and bedding parallel veins do not cross-cut, but have instead developed contemporaneously (Figure 27).

These two scenarios together with the fracture formation model suggests that the bedding parallel veins developed syn- to post-genetically with the conjugate veins, forming an interconnected fracture mesh. Supralithostatic pressurized hydrothermal fluids was forced into developing (horizontal extension) and existing (bedding parallel flexural flow) fractures/weak planes during fold lock up of the Karibib Dome.

3.6 Footwall Ore Distribution

Modelling the FW ore body highlights three major ore trends. Understanding how the ore was distributed and the controlling factors thereto, aims to provide insights into how ore body(ies) evolved.

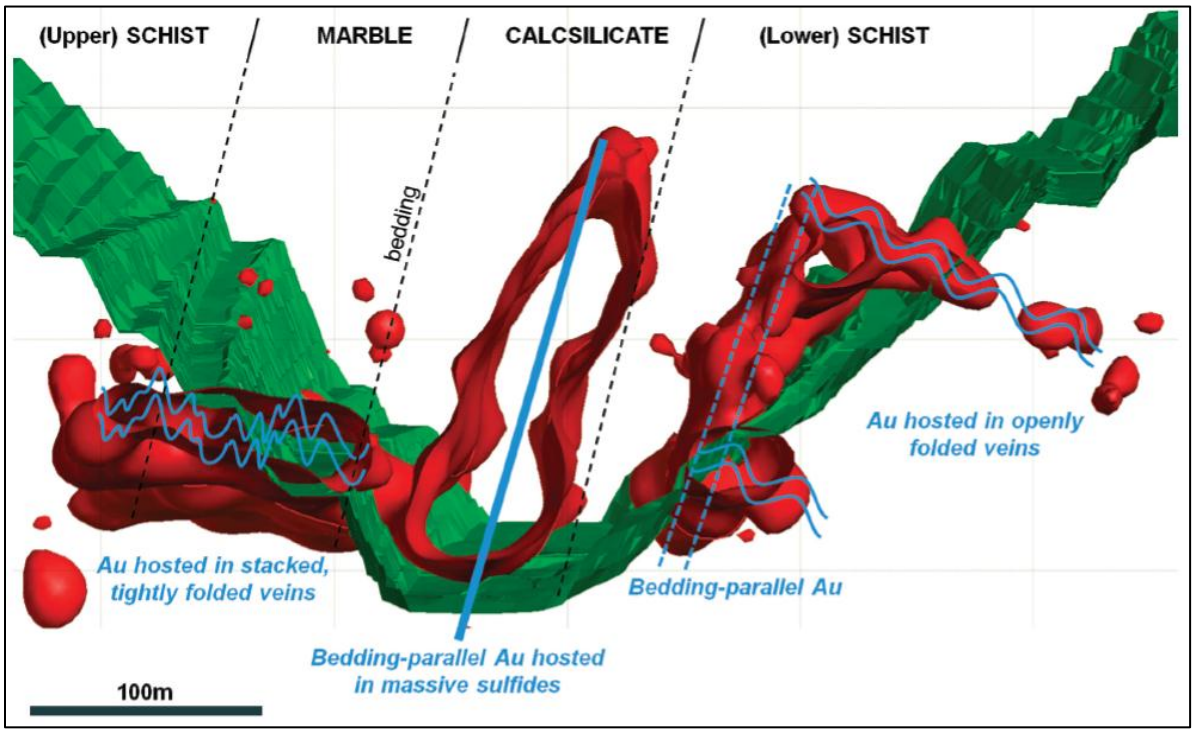

Figure 27: Represents a WNW-ESE cross-section (looking NE) through the central parts of the Navachab Open pit (in green) with the occurring ore zones in red. Note the sub-vertical and sub-horizontal ore trends present in the FW, the lower schist, (after Vollgger et al. 2012)

The three main ore directions observed in the FW trends a) shallowly towards the NE (the down plunge extent), b) sub-vertically along the down plunge extent and c) sub-horizontally across the down plunge extent (Figure 28). The down plunge extent is the most prolific and defines the major trend of the Navachab Gold Deposit. The trend is well documented by Kisters (2005) and Wulff (2008). Kitt (2008) describes its development as follows: The orientation of shallow NE plunging ore shoots identified by exploration and mining corresponds to the intersection of the shallow dipping quartz veins (CVS) with the steeply dipping bedding'. The NE ore plunge is associated with the regional D2 event as the trend is developed parallel to the axial plane of the Karibib Dome.

The sub-vertical and sub–horizontal ore trends are seen as secondary, lower grade bodies developed around the major down plunge extent of the Navachab ore body. Understanding these trends and their controlling factors has become more important as future mining activities are focussed on expanding the main pit to regain access to pit bottom (the high grade down plunge ore extent). These trends evolved as local and regional controls interacted within the FW sequence. This section aims to identify and understand these 'secondary' ore trends, placing emphasis on the local host rock controls and gold grade distribution within different quartz vein sets.

3.6.1 Mineralization within different host rocks

The FW sequence consists primarily of two interbedded sub-units, biotite schists and calc-silicate felses, see section 3.2. This section investigates whether mineralization is favoured to develop within one sub-unit opposed to another thereby identifying a control to the mineralization.

Thirty-one weep holes (Figure 18A) were selected and geologically logged according to sub-unit composition. Differentiation was made between biotite schist and calc-silicate host lithologies within the FW sequence. Zones where the units are interbedded were classified into one of the two sub-units by highest (more than 50%) proportion.

A total of 2862m were logged and assayed for gold content. Fairly equal amounts of sub-units where analysed, as biotite schist made up 1337m (47%) and calc-silicates contributed 1525m or 53% of the total material studied. This meant that the degree of mineralization, hosted by quartz veins, contained in the different sub-units could be compared.

Assay results were returned for each individual 1m sample interval and were classified as mineralized if the result was greater or equal to 0.25g/t (cut-off grade for mineralization). Following a standard industry procedure, sample intervals were clipped at 30g/t to decrease the nugget effect occurring within the deposit. This technique was only applied to 12 samples having a minor effect on the batch results.

After applying the 0.25g/t cut-off, 18.8% or 538m of the material was classified as being mineralized (Table 5). The biotite schists accounted for 11.7% (334m) of the mineralized material while the calc-silicates only contributed 7.2% (205m). The same was done for different cut-offs as the trend persisted to show the schistose units are mineralized much more frequently than the calc-silicates (Table 5).

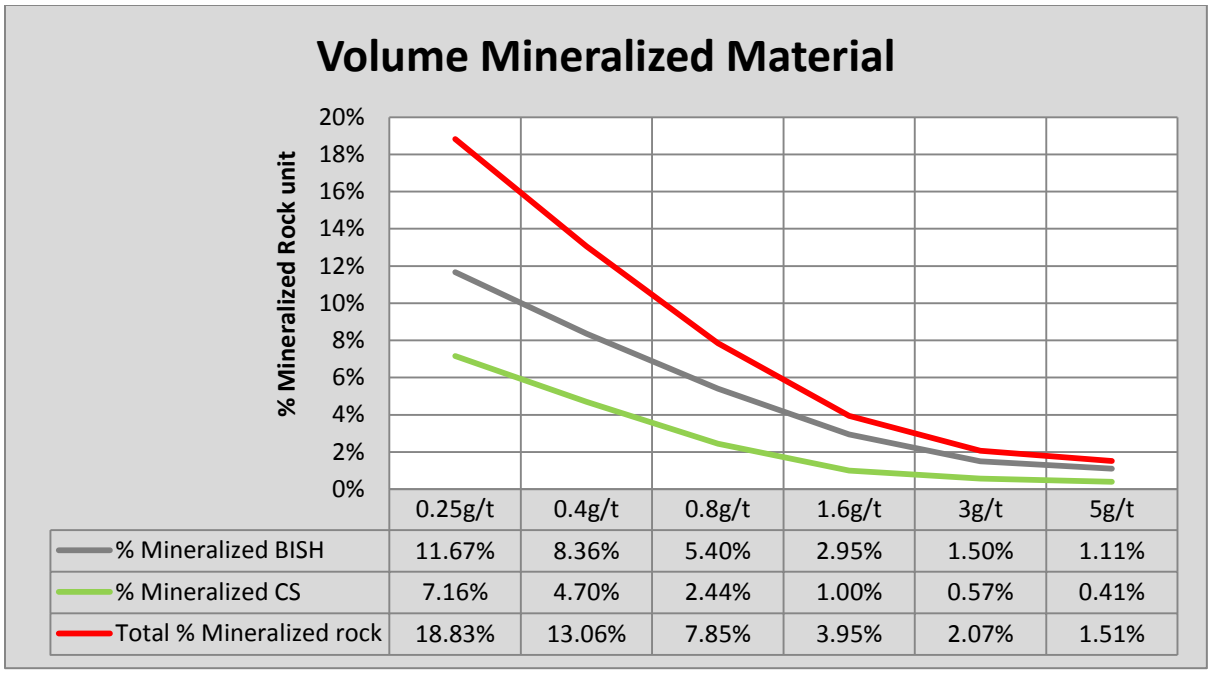

	0.25g/t	0.4g/t	0.8g/t	1.6g/t	3g/t	5g/t
% Mineralized BISH	11.67%	8.36%	5.40%	2.95%	1.50%	1.11%
% Mineralized CS	7.16%	4.70%	2.44%	1.00%	0.57%	0.41%
Total % Mineralized rock	18.83%	13.06%	7.85%	3.95%	2.07%	1.51%

Table 5: the volume % of rock mineralized is compared between calc-silicate felses and biotite schist. The plotted trend highlights the schistose units as having a higher rock volume of mineralized material, thus acting as a better host to quartz vein development within the FW.

The average grades for each cut-off was calculated by determining the amount of gold metal each interval of mineralized sub-unit contained.

$$\boldsymbol{rock\ volume\ (bcm) \times assay\ result\ \left(\frac{g}{t}\right) = Au\ contained\ per\ sample\ interval(g)}$$

$$\boldsymbol{Bank\ Cubic\ Meter\ (bcm) = volume\ of\ rock \times rock\ spesific\ gravity}$$

After filtering the data according to selected cut-off grades, for each sub-unit individually, the combined gold contained from each interval in the filtered out package of rock can be calculated.

$$\boldsymbol{total\ contained\ gold\ (g) per\ cutoff\ interval \div}$$

$$\boldsymbol{total\ rock\ volume\ (bcm\ or\ tons) = average\ grade\ for\ rocks\ within\ cut - off\ (gram\ per\ ton)}$$

Dividing the total contained gold by the contained volume of rock (calculated in BCM) provides an accurate average grade, in grams per ton, of the filtered out rock section.

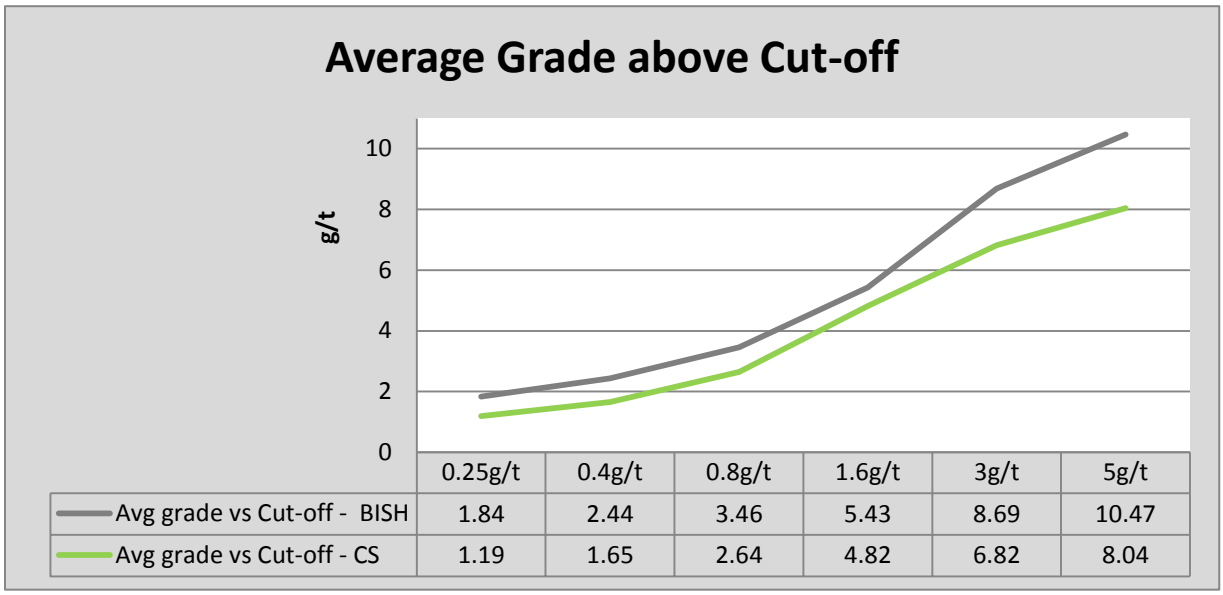

Table 6: shows the average grade for each sub-unit of rock according to different cut-off grades.

The average grade calculations for each cut-off limit highlighted another trend favouring the schistose units as the chief host to mineralization. The biotite schist material contains higher average grades compared to calc-silicate rocks across the same cut-off ranges (Table 6).

3.6.2 Mineralization within different quartz vein sets

The vein sets (CVS, BPV, S2V and other) identified by this study is responsible for bringing about the bulk of the FW mineralization. In establishing the controls to mineralization and how it is distributed throughout the FW, this section aims to establish the best mineralized vein set. The 10 drillholes selected for detailed structural measurements, section 3.4.1, were used. Each interval was considered and only

intervals containing a separate vein were selected. This method allowed for the comparison to be made between different veins and their unique assay result.

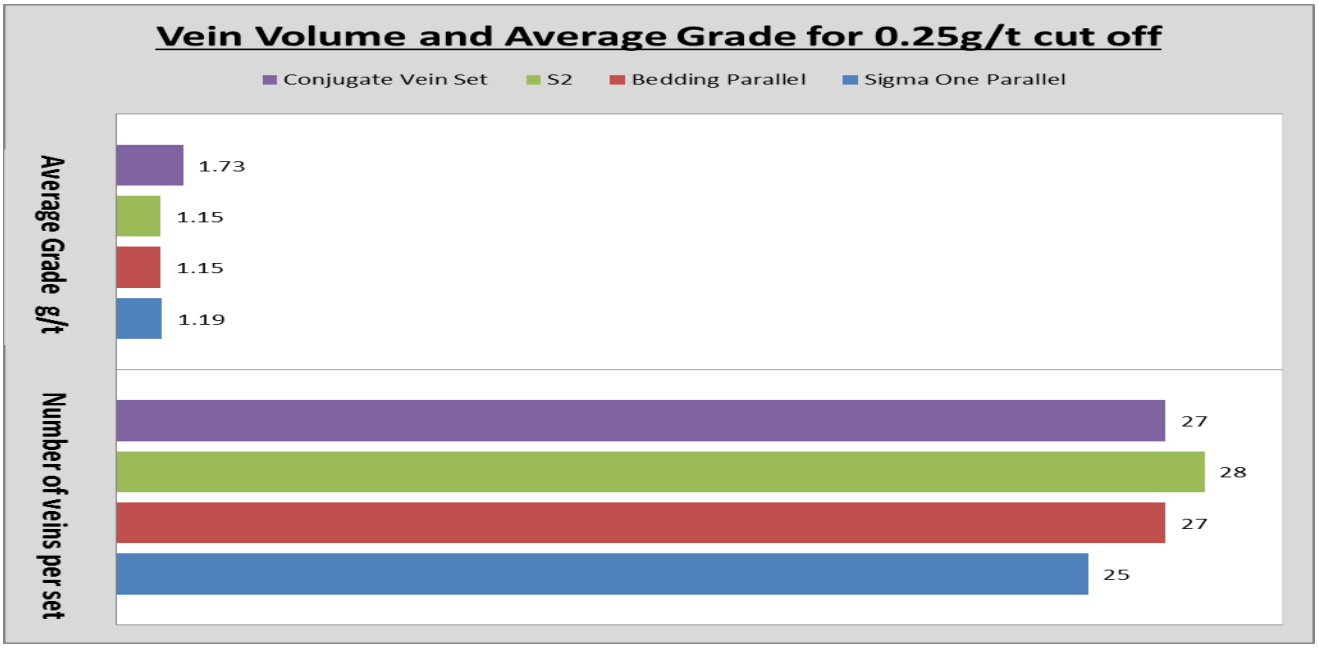

Table 7: The number of veins per set, and average grade of these are plotted. As a similar number of veins were identified for each set, the CVS appears to have the highest average grades.

Due to the abundance of veins cross cutting the FW, the amount of sample intervals conforming to this criterion was rather low. A total of only 107 intervals were identified out of a possible 2862. The number of intervals or veins per vein set was very similar, each constituting about 25% of the total veins identified (Table 7). According to the limited data, the CVS are mineralized at higher average grades compared to the other quartz vein sets found. Upon closer inspection an important bias was identified brought about by the drill orientation. Drilling horizontally will inevitably intersect larger amounts of the sub-horizontally trending CVS (Figure 28) compared to the sub-vertical BPV and S2V's.

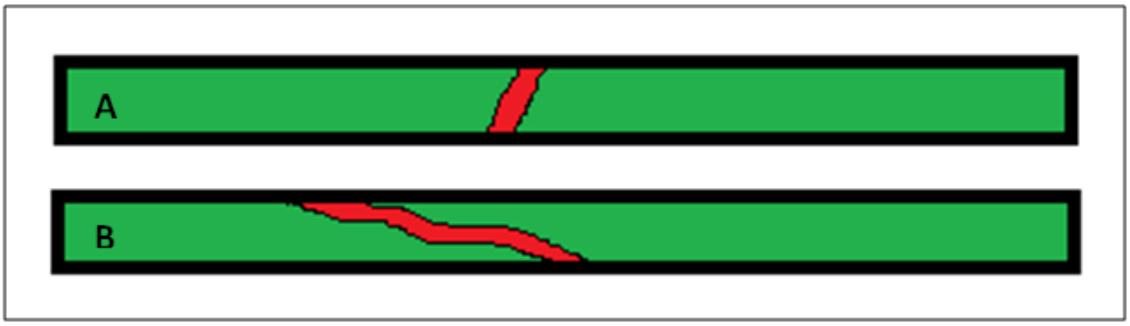

Figure 28: A sketch representing 2 one meter drill intersects containing, in A, a BPV and in B a CVS. The sketch illustrated how drilling sub-parallel to the CVS increases the volume of vein material vs. host rock material for that sample interval. A BPV of similar thickness will have a much higher vein to host rock material ration, influencing the assay result negatively.

A higher volume of vein material per sample interval will positively affect the assay result. The CVS contributed more vein volume to the sample interval possibly resulting in higher average grades being returned while the other vein sets are all equally mineralized.

To remove the vein vs. host rock volume bias, ten veins from each set was sampled by removing all the surrounding host rock material. Veins were also selected to provide similar weights/volumes of material, ranging between 200 to 300 grams. This will test the grade carried by each vein without dilution by the host rocks.

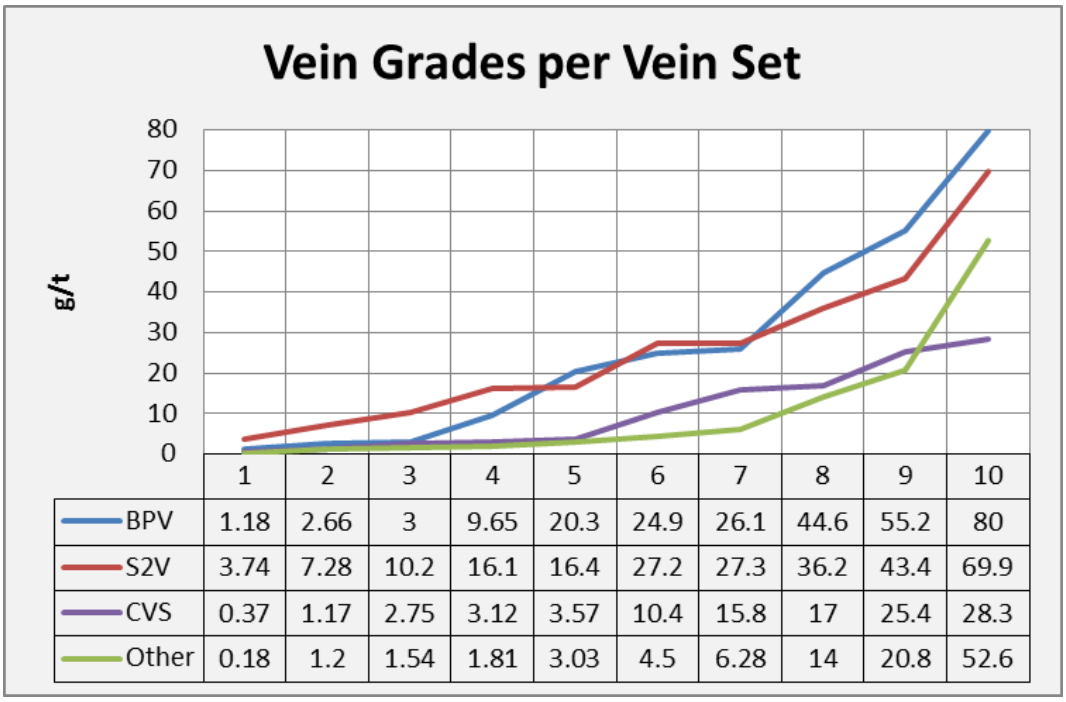

	1	2	3	4	5	6	7	8	9	10
BPV	1.18	2.66	3	9.65	20.3	24.9	26.1	44.6	55.2	80
S2V	3.74	7.28	10.2	16.1	16.4	27.2	27.3	36.2	43.4	69.9
CVS	0.37	1.17	2.75	3.12	3.57	10.4	15.8	17	25.4	28.3
Other	0.18	1.2	1.54	1.81	3.03	4.5	6.28	14	20.8	52.6

Table 8: Grades of different veins from each vein set was assayed. The BPV and S2V returned the highest grades, almost twice that of the CVS.

The assay results were sorted from smallest to largest and plotted on Table 8. The BPV and S2V developed parallel trends as these vein sets returned the highest grades and averages. According to the data the CVS aren't that well mineralized with an average grade of only 10.8g/t while the BPV returned grades of almost twice that.

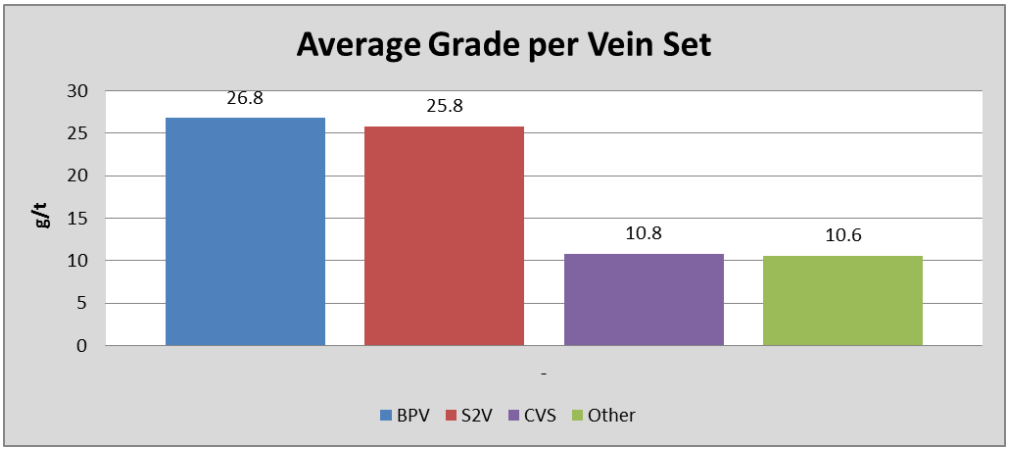

Table 9: Shows the average grades for the 10 veins per vein set, note the high values recorded for the BPV and S2V.

The two data sets (Table 7 and Table 9) show contrasting results, the size of the data sets however doesn't really allow for concrete conclusions to be made. The data does however show all veins are well mineralized and ore zones are controlled by vein abundance rather than vein type.

Chapter 4: Discussion

The development of quartz vein networks result from hydraulic failure in the deeper crust, followed by the influx of large volumes of near-lithostatic pressured fluids (Cox et al. 1991). Fluid flow in the crust is driven by hydraulic gradients (from areas of high mean rock stress to areas with lower mean rock stress) and permeabilities, developed as fracture permeabilities (veins) in the otherwise impermeable host rocks. These controlling factors for fluid flow are determined by tectonic action and deviatoric stresses in the crust. In order to understand how these large hydrothermal vein systems came to be, it is important to investigate the regional structural controls that influence the regional and local hydraulic heads and the permeability evolution of the host rocks (Cox et al. 1991; Ridley, 1993; Sibson and Scott, 1998; Cox et al. 2001).

It is well established that the Navachab mineralized quartz vein network developed during the late stages of the D2 NW-SE directed, sub-horizontal shortening event. Regional structural controls were activated as top-to-the-NW thrusts and NW-verging folds. In the surrounding area the Mon Repos thrust acts as the first order structure interacting with the second order limb of the Karibib dome. The steep NW limb of the dome underwent flexural flow, vertical extension and bedding parallel shearing/faulting as fold amplification and lockup brought about the permeabilities necessary for the in-fluxing hydrothermal fluids.

Gold mineralization has developed in three different orientations throughout the FW sediments. The NE down plunge extent is related to regional controls as it is orientated parallel to the axial plane of the Karibib dome. The sub-parallel and sub-vertical ore

trends are the likely result of interacting regional and local controls facilitating the formation and distribution of the quartz vein sets.

During fold amplification of the Karibib dome, flexural flow resulted in thrust faults developing along bedding contacts of units with contrasting competencies. Fold lock-up followed as regional NW-SE shortening continued, triggering vertical extension along the steeply dipping NW limb. Mean rock stress within the limb was reduced during extension driving over-pressurized hydrothermal fluids into the limb area. The fluids were sucked into sub-horizontally, vertically opened, spaces to produce the conjugate vein set. The S2V followed the dome's axial plane foliation along which fractures developed during the event. Extension further facilitated fluid movement into the pre-existing sub-vertical bedding parallel fault fracture system, following the path of less resistance, which resulted in the bedding parallel veins.

Folding and boudinage observed in the CVS suggest regional shortening and local extension continued after vein emplacement. The occasional cross-cutting relationship between earlier conjugate veins and later bedding parallel veins indicates fluid flow was still active during late shortening. Here fluids were no longer accommodated in horizontally opened spaces as compression was no longer facilitated by extension but rather by thrusting along pre-existing weak planes such as sub-vertical bedding and S2 foliations, both trending parallel to the axial plane of the dome.

The higher gold grades observed within the S2 and BP veins can be explained by 2 scenarios working together or as separate entities.

1) A lower angle orientation to the bedding is more favourable for a vein to propagate fast, not having to cross cut different sub-units, and thus allowing it to take up more fluid/volume per time unit. This becomes especially important if phase separation is assumed as the gold precipitating mechanism since inducing a large pressure drop in the fluid is critical for Au precipitation.

2) These thrusts acted as pathways along which fluids could flux to form the later bedding parallel and S2 veins. Later fluids likely remobilized some of the gold in earlier developed veins, upgraded the gold grades of the later developed bedding parallel and S2 veins.

The eventual conclusion of the D2 shortening event lead to a period of regional extension that activated normal fault action along bedding foliations. These faults would be associated with minor movement that further influenced the distribution of ore zones within the FW package.

Ore distribution

The sub-horizontal ore trend

The ore trend is largely controlled by sheeted conjugate veins developing in clusters, around the down plunge ore extent, across the vertically extended limb. These veins relate to the bedding parallel and S2 sets regarding vein thickness, alteration selvages and emplacement timing. No significant correlation between any of these factors and the Au-grade in the veins was found. Although well mineralized, average gold grades for the CVS appear lower while the amount/volume of conjugate veins contained within the

FW is much higher compared to the bedding parallel and S2 veins. The dataset used to obtain average grades for the different veins sets, by removing all host rock thus eliminating the effect of dilution, is small and may not fully represent the study area, further investigation is required. This study did however find that the volume of conjugate veins developed across the FW sequence makes this the dominant gold hosting vein set.

Another finding was that the biotite schist units contains a higher volume of quartz veins compared to that developed in the calc-silicate felses. Vein/fracture development is likely favouring the schists as they are less competent than the calc-silicate felses. The schist units are also mineralized at higher average grades compared to the felses. This feature is again related to differences in competencies between the host rocks as faster opening fractures likely resulted in higher amounts of gold precipitating within veins.

The sub-vertical ore trend

Fractures/weak planes developed as the Karibib dome was progressively folded. These fractures resulted from thrust action as flexural flow occurred along bedding units within the NW limb of the dome. Over pressurized fluids were then forced into these permabilities bringing about the bedding parallel quartz veins. The S2 veins emplaced during fold lockup, as described above, and add value to the sub-vertical ore trend. The S2 and bedding parallel veins have higher gold grades compared to the CVS, as deducted from a small but meaningful dataset.

Host rock composition acts as a local control as the biotite schists are more susceptible to fracture forming and vein hosting than the calc-silicate units. Two factors might be aiding fracture development within the schists as (1) they are less competent (explained

above) and (2) faulting, leading to fracturing, will be facilitated along the bedding parallel schistosity developed within the rocks.

Additional control

Another observation influencing ore distribution is displacement. As faulting occurred during and after the D2 event, mineralization was displaced within the FW. The exact magnitude and orientation of displacement requires further investigation, but it is suggested that faulting occurred predominantly along a sub-vertical trend, parallel to bedding. Faulting observed within the main pit also suggest later faults cross cutting bedding at higher angles.

These observations highlight the interaction of regional structural and local lithological controls as they determine where quartz veins emplaced and where they are redistributed to across the FW.

Mineralisation Model

It is evident from this study and previous works that the late stages of the D2 shortening event is largely responsible for bringing about the fluid plumbing system responsible for the Navachab Gold deposit. In addition, the convergent and collisional tectonics activated metamorphic dehydration of the buried meta-pelites, Figure 29. Gold was introduced to the system either by a magmatic or paleo-placer source developed at mid to upper crustal levels. As these hydrothermal fluids fluxed it allowed them to absorb this in-situ Au and transport it in solution to higher crustal levels. Fluid movement was primarily facilitated by the activation of 1st order structures e.g. shearing of the steep NW limb of the Karibib Dome, especially along the Spes Bona and Okawayo contact,

the Mon Repos Thrust Zone and possible blind thrusts. With continued deformation and interaction of the structures an extensional stress field developed along the NW limb of the Karibib Dome. Extension lowered mean rock stress allowing gold saturated hydrothermal fluids to be sucked in and fill opening fractures while gold precipitated as fluid pressure decreased.

Two important local controls facilitated vein formation and distribution within the FW sequence. Biotite schists were established as the favoured host rocks to well mineralised veins and 2) local faulting/shearing along steep lithologies on the NW limb facilitated sub-vertical vein formation while displacing sub-horizontal ore zones sub-vertically.

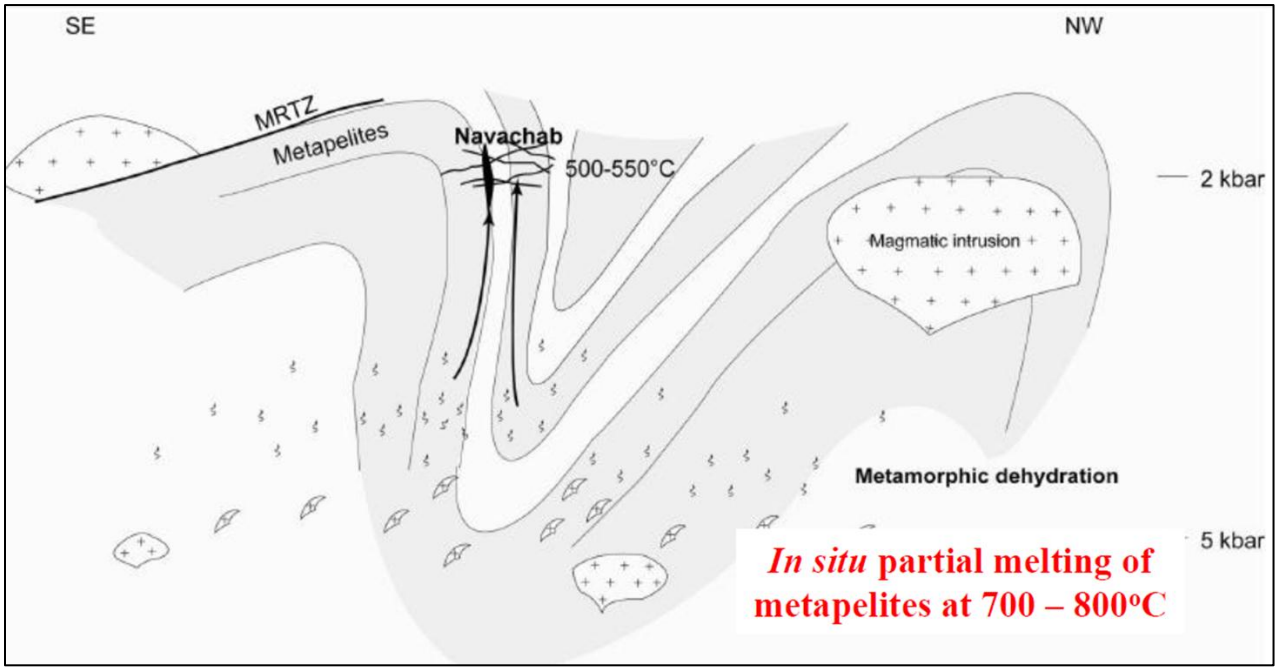

Figure 29: The mineralisation model (Steven et al., 2014) explains how metamorphic dehydrated resulted in the release of fluids. Collisional tectonics further facilitated the development of primary fluid path ways transporting the enriched fluids to a deposit scale. Here hydrothermal fluids reacted with fluid sinks such as a physical throttle and/or a chemical trap, allowing gold to precipitate from solution.

The mineralisation model (Figure 29) shows the dehydration of metapelites at depth and accumulation of the resulting fluids in above mentioned 1st order structures, the primary active fluid path ways. This gold enriched, ascending, hydrothermal fluids reacted with fluid sinks (related to a physical throttle and/or a chemical trap) to precipitate gold from solution at a deposit-scale. Regarding the footwall ores, these physical throttles (local controls mentioned above) were identified as 1) folding and fold lock-up resulting in crustal extension reducing mean rock stress to allow the influx of fluids, 2) the brittle schist fracturing more readily by being less competent than the calc-silicates and 3) fracture development along steep bedding and bedding parallel shears allow increased fluid flux as fractures open to decrease fluid pressure and precipitate gold.

Chapter 5: Conclusion

This section concludes on the aims set out earlier in the write-up.

Host Rock

The study found that 18.8% of the host rock investigated is mineralized at an average grade of 1.5g/t and a grade cut-off at 0.25g/t. The biotite schist units play host to 11.7% of the mineralization while only 7.1% is developed within the calc-silicate felses. Average gold grades for the mineralized schist above the 0.25g/t cut-off was calculated at 1.84g/t and 1.19g/t for the felses. To conclude, the biotite schist units contain a larger volume amount (61% more) of quartz veins and these are mineralized at higher (64%) average gold grades compared to the calc-silicate sub-units of the FW sequence.

Quartz Vein Sets

1456 quartz-sulphide veins, from 10 weep holes, were structurally measured and the data interpreted by stereographic projections. The three main quartz vein sets identified in the FW sequence are:

1. A conjugate vein set (CVS) consisting of 2 main vein arrays with shallow dips (between 5˚ and 40˚) towards the NE and NW respectively,
2. a set of steeply (56-89°) WNW-dipping, bedding/foliation parallel veins (BPV) with an average dip direction of 293˚/75˚ and
3. a S2 fold (Karibib dome) axial planar vein set (S2V) dipping steeply (75-89°) towards the SE

By merging historic vein orientation data with data from this study a combined dataset was developed consist of 1351 quartz vein. The conjugate quartz vein set (CVS)

constitutes 38% (531 veins) of the total number of veins measured, the bedding parallel (BPV) veins 22% (300 veins) and the S2V with 17% (229 veins). All other veins with unrecognised orientations contribute to 22% (291 veins) of the total veins measured in the FW.

Ten veins of each vein set were stripped off any host rock, eliminating dilution, and assayed for gold content. Although small, the dataset showed that the BPV and S2V have average grades of almost 2.5 times more than the CVS. The result can be explained by continued activation along sub-vertical fractures after the CVS formed, remobilising some of the gold contained and upgrading grades in the later developed BPV and S2V. Another reason can be ascribed to the sub-vertical veins forming within certain sub-units. This resulted in the rapid opening of fractures allowing higher fluid flux and pressure changes to facilitating gold precipitation. The S2 and BP veins appear to be mineralized at higher grades, but the sheer volume of CVS contained within the FW makes the set the dominant host of the FW mineralization.

Displacement

Faulting is observed on all scales in and around the main pit occurring primarily along bedding foliations and secondly at higher angles across the foliation. The study did not investigate the extent of the displacement but can conclude that it is a prominent control to ore distribution across the FW, especially along the sub-vertical trend.

Summary of the mineralization controls

The Navachab gold mineralisation came about as a result of convergent and collisional tectonics activating metamorphic dehydration of the host rocks in the area. As these

fluids moved they absorbed gold from the crust (metapelites), emplaced by either a magmatic or paleo-placer source. The gold enriched hydrothermal fluids amalgamated in large scale 1ste order structures (shearing of the steep NW limb of the Karibib Dome, the Mon Repos Thrust Zone) that acted as primary active fluid path ways. In the case of Navachab the gold enriched fluid fluxed along these pathways while interacting with fluid sinks related to a physical throttle (brittle schist, folding, steep bedding and bedding parallel shears, competency contrast between schists and marbles) and/or a chemical trap (marbles). Following the fluid sinks and active fluid pathways identified by this and previous works, it is strongly recommended that a detailed mineral approach system be designed and implemented to lead future exploration endeavours.

Recommendations

Developing a mineral system approach, McCuaig et al., (2009), as targeting model presents advantages over the empirical exploration approaches, or deposit model approach traditionally used. The mineral system approach has a basis in probability theory and is accommodating enough to allow for the discovery of a new style of deposit, rather than just analogues of what have already been found.

The mineral system approach relies on the breakup of the mineralising process into a series of fundamental critical processes that can be treated as independent variables. These range from a primary fluid source region, an active fluid pathway, and at the deposit-scale a fluid sink related to a physical throttle and/or a chemical trap (Figure 30).

The critical process termed a “physical throttle” corresponds to the mechanism by which the fluid flow is affected by constriction or obstruction. Typically this critical process is associated with constituent processes of two sorts. The first one regroups typical structural features such as fault intersections, bends along major structures, relay faults and can be grouped as “breach settings”. The second of these constituent processes can be regrouped under the generic term of “seals” or an impermeable barrier (physical or chemical) that cap or obstruct the fluid flow along its fluid pathways, allowing fluid to be focused through the breach zones.

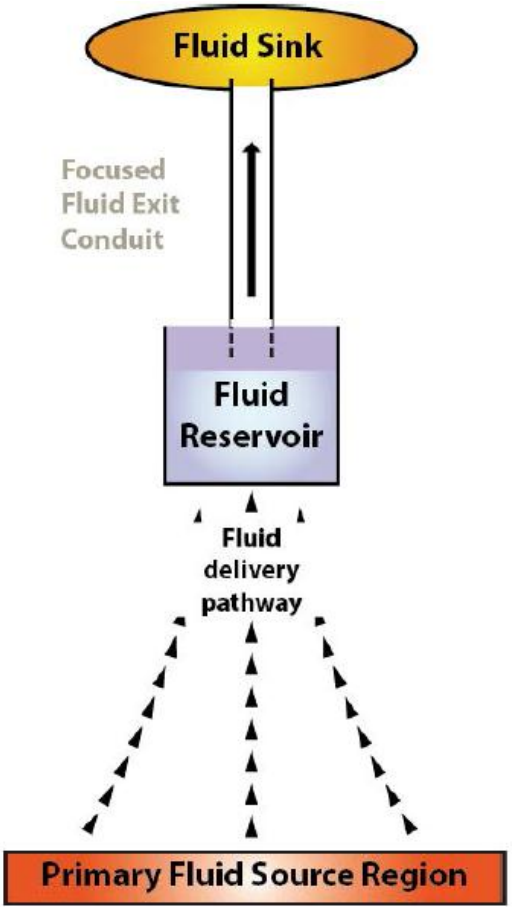

Figure 30: Figure showing the mineral system concept for the development of ore deposits (after Hronsky et al., 2010)

The Chemical Scrubber describes the physical and/or chemical process by which gold complexes in the fluid phase are destabilized allowing the deposition of gold (marbles, black shales etc.). Note that while Active Pathway and Physical Throttle critical processes are essentially associated with regional structural architecture and can be derived from the compilation of the potential field data and geological data. The identification of the chemical scrubber process strongly relies on the availability of a regional geochemical (multi-element) data set.

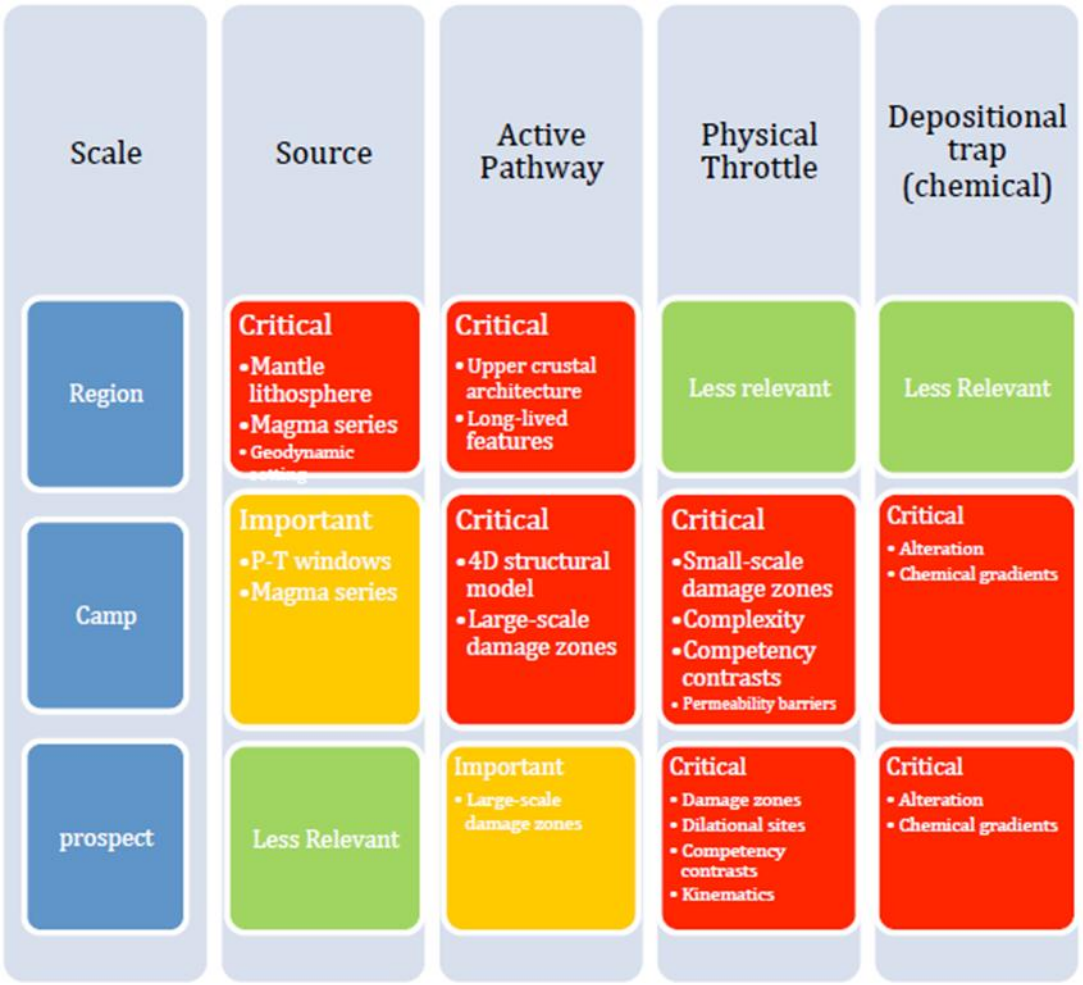

Figure 31: Presents the scale dependant targeting criteria for most orogenic gold processes (after McCuaig et al., 2009)

The resulting targeting model derived from a mineral system approach relies on the definition of: (1) critical processes which correspond to the primary features of the mineral system (i.e. Active Pathways, Physical Throttles and Chemical Traps), (2) constituent processes which represent the variety of ways that can cause the critical process to happen, and (3) targeting element /proxies which are mappable features that can be readily queried in the available geological dataset (i.e. what data set is then used to do physical targeting on the ground). This approach is synthesized on figure 31.

Chapter 6: Reference List

Anderson, H.F. Nash, C.R. (1997) Integrated lithostructural mapping of the Rössing area, Namibia, using high resolution aeromagnetic, radiometric, Landsat data and aerial photographs. Exploration geophysics 28, 185-191.

Badenhorst, F.P. (1987). Lithostratigraphy of the Damara Sequence in the Omaruru Area of the northern Central Zone of the Damaran Orogen and a proposed correlation across the Omaruru Lineament. Communications of the Geological Survey of South West Africa, 3, 3-8.

Badenhorst, F.P. (1992). The Lithostratigraphy of area 2115B and D in the Central Zone of the Damara Orogen in Namibia: with emphasis on facies changes and correlation. Unpublished MSc thesis, University of Port Elizabeth, p. 124.

Barnes, S.J., Sawyer, E.W. (1980) An alternative model for continental convergence. Precambrian Research 13, 297-336.

Blaxland, A., Gohn, E., Haack, U., Hoffer, E. (1979) Rb/Sr ages of late-tectonic granites in the Damara orogen, South West Africa/Namibia. Neues Jahrbuch für Mineralogie, Monatshefte 11, 498.

Bowden, P., Tack, L., Williams, I.S., Deblond, A. (1999) Transpressional and transtensional magmatism in the Central Damaran (Pan-African) orogenic belt, Western Namibia. Abstracts, GSA 11: Earth Resources for Africa. Journal of African Earth Sciences 28, 13.

Brandt, R. (1985). Preliminary report on the stratigraphy of the Damara Sequence and the geology and geochemistry of Damaran granites in an area between Walvis Bay and Karibib. Communications of the Geological Survey of Namibia, 1, 31-43.

Brandt, R. (1987). A revised stratigraphy for the Abbabis Complex in the Abbabis inlier Namibia. South African Journal of Geology, 90, 314-323.

Corner, B. (2000) Crustal framework of Namibia derived from magnetic and gravity data. Communications of the Geological Survey of Namibia 12, 13-20.

Corner, B. (1983) An interpretation of the aeromagnetic data covering the western portion of the Damara Orogen in South West Africa/Namibia. In: Miller, R. McG. (Ed.), Evolution of the Damara Orogen of South West Africa/Namibia. Special Publications of the Geological Society of South Africa 11, 339–354.

Cox, S., Wall, V.J., Etheridge, M.A., and Potter T.F. (1991). Deformation and metamorphic processes in the formation of mesothermal vein-hosted gold deposits – examples from the Lachlan fold belt in central Victoria, Australia. Ore Geology Reviews, 6, 391-423.

Cox, S.F., Sun, S.-S., Etheridge, M.A., Wall, V.J., and Potter T.F. (1995). Structural and geochemical controls on the development of turbidite-hosted gold quartz vein deposits, Wattle Gully mine, central Victoria, Australia. Economic Geology, 90, 1722-1746.

Cox, S.F., Knackstedt, M.A., Braun, J., (2001). Principles of structural control on permeability and fluid flow in hydrothermal systems. In: Richards, J.P., Tosdal, R.M. (Eds.), Structural Controls on Ore Genesis. Reviews in Economic Geology, p. 1–24.

De Kock, G.S. (1989) A geotectonic study of the Damara orogen in an area southeast of Karibib, South-West Africa. Ph.D.-thesis (unpublished), University of the Orange Free State, Bloemfontein, South Africa. 438p.

De Kock, G.S., Eglington B., Armstrong R.A., Harmer, R.E. and Walraven, F. (2000). U-Pb and Pb-Pb ages on the Naaupoort rhyolite, Kawakeup leptite and Okangava Diorite: implication for the onset of rifting and orogenesis in the Damara belt Namibia. Communications of the Geological Survey of Namibia, 12, 81-88.

De Kock, G.S. (2001) A reappraisal of the Namibian Damara stratigraphy in part of the Southern Swakop Terrane and its implications to basin evolution. South African Journal of Geology 104, 115-136.

Downing, K.N., Coward, M.P. (1981) The Okahandja Linearment and its significance for Damaran Tectonics in South West Africa. Geologische Rundschau 70, 972-1000.

Etheridge, M.A., (1983). Differential stress magnitudes during regional deformation and metamorphism: upper bound imposed by tensile fracturing. Geology, 1, 231–234.

Goldfarb, R.J., Groves, D.I., Gardoll, S., (2001). Orogenic gold and geological time: a global synthesis. Ore Geology Reviews, 18, 1-75.

Gray, D.R., Foster, D.A., Goscombe, B., Passchier, C.W. & Trouw, R.A.J. (2006). 40Ar/39Ar thermochronology of the Pan-African Damara Orogen, Namibia, with implications for tectonothermal and geodynamic evolution. Precambrian Research, 150, 49–72.

Gray, D.R., Foster, D.A., Meert, J.G., Goscombe, B.D., Armstrong, R., Trouw, R.A.J., Passchier, C.W. (2008) A Damara orogen perspective on the assembly of southwestern Gondwana. Geological society of London, Special publications 294, 257-278.

Groves, D.I., Goldfarb, R.J., Gebre-Mariuam, M., Hagemann, S., Robert, F. (1998). Orogenic gold deposits: A proposed classification in the context of the crustal distribution and relationship to other gold deposit types. Ore Geology Reviews, 13, 7-28.

Groves, D.I., Goldfarb, R.J., Robert, F., Hart, C.J.R. (2003). Gold deposits in metamorphic belts: overview of current understanding, outstanding problems, future research and exploration significance. Economic Geology, 98, 1-29.

Hodgson, C.J. (1989). The structure of shear-related, vein-type gold deposits: a review. Ore Geology Reviews, 4, 231-273.

Hawkesworth, C.J., Marlow, A.G. (1983) Isotope Evolution of the Damara orogenic belt. In: Miller, R.McG. (Ed), Evolution of the Damara Orogen of South West Africa. Special Publication of the Geological Society of South Africa 11, 397-408.

Henry, G. (1992) The sedimentary evolution of the Damara Sequence in the lower Khan River valley, Namibia. PhD thesis, University of the Witwatersrand, Johannesburg, South Africa.

Hodgson, C.J. (1989). The structure of shear-related, vein-type gold deposits: a review. Ore Geology Reviews, 4, 231-273.

Hoffmann, C., (1976) Granites and migmatites of the Damara belt, South West Africa. Petrography and melting experiments. International journal of Earth sciences 65, p939-966.

Hoffman. P.F., Hawkins, D.P., Isachsen, C.E. and Bowring, S.A. (1996). Precise U-Pb zircon ages for early Damaran magmatism in the Summas Mountains and Welwitschia inlier, northern Damara belt, Namibia. Communications of the Geological Survey of Namibia, 11, 47-52.

Hoffmann, K.-H., Condon, D.J., Bowring, S.A. and Crowley, J.L. (2004). U-Pb zircon date from the Neoproterozoic Ghaub Formation, Namibia: Constraints on Marinoan glaciation. Geology, 32, 817-820.

Jacob, R.E. (1974). Geology and metamorphic petrology of part of the Damara Orogen along the lower Swakop River, South West Africa. Bull. Precambrian Res. Unit, Univ. Cape Town, 17, p. 184.

Jacob, R.E., Kroner, A. and Burger, A.J. (1978). Areal extent and first U-Pb age of Pre-Damaran Abbabis Complex in the Central Damaran belt of South West Africa. Geologische Rundschau, 67, 706-718.

Jacob, R.E., Snowden, P.A. and Bunting, F.J.L. (1983). Geology and structural development of the Tumas Basement Dome and its cover rocks. In: Miller, R.McG. (Ed), Evolution of the Damara Orogen of South West Africa. Special Publication of the Geological Society of South Africa, 11, 157-172.

Jacob, R.E., Moore, J.M. and Armstrong, R.A. (2000). Zircon and titanite age determinations from igneous rocks in the Karibib District, Namibia: implications for Navachab vein-style gold mineralization. Communications of the Geological Survey of Namibia, 12, 157-166.

Johnson, S.D. (2005). Structural geology of the Usakos dome, Damara Belt, central Namibia. Unpublished MSc thesis, University of Stellenbosch, p. 159.

Johnson, S.D., Poujol, M., Kisters, A.F.M. (2006) Constraining the timing and migration of collisional tectonics in the Damara Belt, Namibia: U-Pb zircon ages for the syntectonic Salem-type Stinkbank granite. South African Journal of Geology 109 427-440.

Jung, S. and Mezger, K. (2003). Petrology of basement-dominated terranes: I Regional metamorphic T-t path from U-Pb monazite and Sm-Nd garnet geochronology (Central Damara orogen, Namibia). Chemical Geology, 198, 223-247.

Jung, S., Hoernes, S., Mezger, K. (2002) Synorogenic melting of mafic lower crust: constraints from geochronology, petrology and Sr, Nd, Pb and O isotope geochemistry of quartz diorites (Damara orogen, Namibia). Contributions to Mineral Petrology 143, 551-566.

Jung, S., Hoernes, S., Mezger, K. (2001) Trace element and isotopic (Sr, Nd, Pb, O) arguments for a mid-crustal origin of Pan-African garnet-bearing S-type granites from the Damara orogen (Namibia). Precambrian Research 110, 325-355.

Jung, S., (2000) High-temperature, mid-pressure clockwise P–T paths and melting in the development of regional migmatites: the role of crustal thickening and repeated plutonism. Geological Journal 35,345-359.

Jung, S., Hoernes, S., Masberg, P., Hoffer, E. (1999) The petrogenesis of some migmatites and granites (Central Damara orogen, Namibia): Evidence for disequilibrium melting, Wall rock contamination and crystal fractionation. Journal of petrology 40, 1241-1269.

Kasch, K.W. (1983a) Continental Collision, Suture Progradation and Thermal Relaxation: A Plate Tectonic Model for the Damara Orogen in Central Namibia. In: Miller, R.McG. (Ed.), Evolution of the Damara Orogen of South West Africa. Geological Society of South Africa, Special Publication 11, 423-429.

Kerrich, R., Goldfarb, R.J., Groves, D.I., Garwin, S. (2000). The geodynamics of world-class gold deposits: Characteristics, space-time distributionh and origins. In: Hagemann, S. and Brown, P.E. (eds.) Gold in 2000. Reviews in Economic Geology, pp.501-551.

Kisters, A.F.M., Smith Jordaan, L. and Neumaier, K. (2004). Thrust-related dome structures in the Karibib district and the origin of orthogonal fabric domains in the south Central Zone of the Pan-African Damara belt, Namibia. Precambrian Research, 133, 283-303.

Kisters, A.F.M. (2005). Controls of gold-quartz vein formation during regional folding in amphibolite-facies, marble-dominated metasediments of the Navachab Gold Mine, in the Pan-African Damara Belt, Namibia. South African Journal of Geology. 108, 365-380.
Kitt, S. (2008). Structural controles of Auriferous Quartz veins in the Karibib Area, South central zone of the Pan-African Damara Belt, Namibia

Kolb J (2008) The role of fluids in partitioning brittle deformation and ductile creep in auriferous shear zones between 500 and 700°C. Tectonophysics 446: 1-15

Kukla, P.A., Opitz, C., Stanistreet, I.G., Charlesworth, E.G. (1988) New aspects of the sedimentology and structure of the Kuiseb Formation in the western Khomas Trough, Damara Orogen, SWA/Namibia. Communications of the geological survey of Namibia 4, 33-42.

Kukla, P.A., Stanistreet, I.G. (1991) Record of the Damaran Khomas Hochland accretionary prism in central Namibia: refutation of an ensialic origin of the late Proterozoic orogenic belt. Geology 19, 473–476.

Martin, H., (1965) The Precambrian geology of South West Africa and Namaqualand. Bulletin of the Precambrian research unit, University of Cape Town, 4, 1-159.

Martin, H., Porada, H. (1977) The intracratonic branch of the Damara orogen in South West Africa. I. Discussions of geodynamic models. Precambrian Research 5, 311-338.

Masberg, H.P., Hoffer, E., Hoernes, S. (1992). Microfabrics indicating granulite-facies metamorphism in the low-pressure central Damara orogen Namibia. Precambrian Research. 55, 243–257.

Masberg, H.P. (2000). Garnet grovolumeh in medium pressure granulite-facies metapelites from the central Damara Orogen: igneous versus metamorphic history. Communications of the Geological Survey of Namibia, 12, 115-124.

McCuaig, T.C., Beresford, S.W. (2009) The scale dependency of targeting criteria based on recent advances in understanding mineral systems. In : Proceedings of the 10th Biennial Meeting of the Society for Geology Applied to Mineral Deposits. Townsville, Australia. pp. 123-125.

Miller, R.McG. Hoffmann, K-H. (1981) Guide to the excursion through the Damara orogen. Geological Society of South Africa, Geocongress ’81, 115p.

Miller, R. McG. (1983). The Pan-African Damara Orogen of South West Africa/ Namibia. In: Miller, R.McG. (Ed.), Evolution of the Damara Orogen of South West Africa. Geological Society of South Africa, Special Publication, 11, 431-515.

Miller, R.McG. (2008) The Geology of Namibia. Windhoek, Namibia: Ministry of Mines and Energy, Geological survey.

Moore, J.M. and Jacob, R.E. (1998). The Navachab sheeted vein/skarn Au deposit, Namibia. Abstract volume, Annual Conference of the Geological and Mineralogical Associations of Canada, A125-A126.

Moore, J.M., Jacob, R.E., Harris, C. and Armstrong, R.A. (1999). The Navachab gold deposit, Namibia: a mesothermal sheeted-vein/skarn system related to the Pan-African Damara Orogen. Journal of African Earth Sciences, 28, 50-51.

Nex P.A.M., Oliver, G.J.H. and Kinnaird, J. (2001). Spinel-bearing assemblages and P-T-t evolution of the Central Zone of the Damara Orogen, Namibia. Journal of African Earth Sciences, 32, 471-489.

Nortemann, M.F.-J., Mucke, A., Weber, K., Meinert, L.D., (2000). Mineralogy of the Navachab skarn deposit, Namibia: an unusual Au-bearing skarn in highgrade metamorphic rocks. Communications of the Geological Survey of Namibia, 12, 149–156.

Oliver, G.J.H., (1994) Mid-crustal detachments zones in the central zone of the Damara orogen. Namibia. Journal of African Earth Sciences 19, 331-344.

Piranjo, F. and Jacob, R.E, (1991). Gold mineralization in the intracontinental branch of

the Damara orogen, Namibia: a preliminary survey. Journal of African Earth Sciences, 13, 305-311.

Poli, L.C., Oliver, G.J.H. (2001) Constrictional deformation in the Central Zone of the Damara Orogen Namibia. Journal of African Earth Sciences 33, 303–312.

Porada, H. (1989) Pan-African rifting and orogenesis in southern to equatorial Africa and eastern Brazil, Precambrian Research 44, 103-138.

Porada, H., Wittig, R. (1983) Turbidites and their significance for the geosynclinals evolution of the Damara orogen, South West Africa/Namibia. In: Miller, R.McG. (Ed.), Evolution of the Damara Orogen of South West Africa. Geological Society of South Africa, Special Publication 11, 21-36.

Prave, A.R. (1996). Tale of three cratons: Tectonostratigraphic anatomy of the Damara orogen in northwestern Namibia and the assembly of Gondwana. Geology, 24, 1115-1118.

Puhan, D. (1983). Temperature and pressure of metamorphism in the central Damara orogen. In: Miller, R. McG. (Ed.), Evolution of the Damara Orogen of South West Africa/Namibia. Geological Society of South Africa, Special Publication, vol. 11, 219–223.

Ridley, J.R. (1993). The relations between mean rock stress and fluid flow in the crust: With reference to vein- and lode-style gold deposits. Ore Geology Reviews, 8, 23-37.

Ridley, J. and Mengler, F. (2000). Lithological and structural controls on the form and setting of vein stockwork orebodies at the Mount Charlotte gold deposit, Kalgoorlie. Economic Geology, 95, 85-98.

Robert, F. and Poulsen, K.H. (2001). Vein Formation and deformation in greenstone gold deposits. Reviews in Economic Geology, 14, 111-155.

Sawyer, E.W. (1981) Damaran structural and metamorphic geology of an area south-east of Walvis Bay, SWA/Namibia. Memoir of the Geological Survey of South West Africa/Namibia 7, 94p.

Schaubs, P.M. and Wilson, C.J.L. (2002). The relative roles of folding and faulting in controlling gold mineralization along the Deborah anticline, Bendigo, Victoria, Australia. Economic Geology, 97, 351-370.

Sibson, R.H., Robert, F. and Poulsen, K.H. (1988). High-angle reverse faults, fluid pressure cycling and mesothermal gold-quartz deposits. Geology, 16, 551-555.

Sibson, R.H. (1996). Structural permeability of fluid-driven fault-fracture meshes. Journal of Structural Geology, 18, 1031-1042.

Sibson, R.H. and Scott, J. (1998). Stress/fault controls on the containment and release of overpressurized fluids: Examples from gold-quartz vein systems in Juneau, Alaska; Victoria, Australia; and Otago, New Zealand. Ore Geology Reviews, 13, 293-306.

Sibson, R.H. (2001). Seismogenic framework for hydrothermal transport and ore deposition. Reviews in Economic Geology, 14, 25-50.

Smith, D.A.M. (1965) The geology of an area around the Khan and Swakop Rivers in South West Africa. Memoir of the Geological Society of South Africa, South West Africa Series 3, 113p. 138

Smith, D.A.M. (1966) Geological Map of area 2215B-Usakos, Geological Survey, Windhoek, South West Africa.

Stanistreet, I.G., Kukla, P.A., Henry, G. (1991). Sedimentary basinal responses to a Late Precambrian Wilson Cycle: The Damara Orogen and Nama Foreland, Namibia. Journal of African Earth Science 13, 141-156.

Steven, N.M. (1993). A study of Epigenetic Mineralization in the Central Zone of the Damara Orogen, Namibia, with special reference to gold, tungsten, tin and rare elements. Memoirs of the Geological Survey of Namibia, 16, p. 166.

Steven, N.M. and Badenhorst, F.P. (2002). Mesothermal gold deposits of the Damara Orogen. Excursion guidebook, 11th Quadrennial IAGOD Symposium and Geocongress, Windhoek, p. 225.

Steven, N.M., Wulff, K. and Kisters, A. (2014). Geochronology of the Navachab orogenic gold deposit, Namibia. Roy Miller Symposium Presentation and Abstract, August 2014.

Tack, L., Bowden, P. (1999) Post-collisional granite magmatism in the central Damara (Pan-African) Orogenic belt, western Namibia. Journal of African Earth Science 28, 653–674.

Trompette, R. (1997). Neoproterozoic (~600 Ma) aggregation of westernGondwana: a tentative scenario. Precambrian Research. 82, 101–112.

Trompette, R. (2000) Gondwana evolution: its assembly at around 600Ma. Earth and planetary sciences 330, 305-315.

Vollgger, S.A., Cruden, A.R., Cowan, J.E. (2012) Structural Geology Meets 3D Implicit Deposit Modelling

Ward, R.A., Stevens, G., Kisters, A.F.M. (2008) Fluid and deformation induced partial melting and melt volumes in low-temperature granulite-facies metasediments, Damara Belt, Namibia. Lithos 105, 253-271 .

Windh, J. (1995). Saddle reef and related gold mineralization, Hill End gold field, Australia: evolution of an auriferous vein system during progressive deformation. Economic Geology, 90, 1764-1774.

Wulff, K. (2008). Petrography, geochemistry and stable isotope characteristics of the Navachab gold deposit, Namibia. Unpublished Phd thesis, RVOLUMEH Aachen, Germany, p.
190.

Website: www.earth.google.com